AMERICAN UNIVERSITY OF BEIRUT

TOWARDS IMPROVING WEATHER FORECASTS FOR BEIRUT USING THE COUPLED WRF-UCM

by
MOHAMAD KHEIR GHADBAN

A thesis
submitted in partial fulfillment of the requirements
for the degree of Master of Engineering
to the Department of Mechanical Engineering
of the Maroun Semaan Faculty of Engineering and Architecture
at the American University of Beirut

Beirut, Lebanon
December 2018

AMERICAN UNIVERSITY OF BEIRUT

TOWARDS IMPROVING WEATHER FORECASTS FOR

BEIRUT USING THE COUPLED WRF-UCM
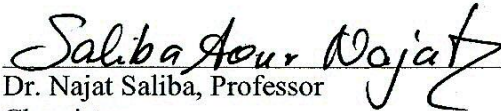
by
MOHAMAD KHEIR GHADBAN

Approved by:

_____

Dr. Issam Lakkis, Professor   Advisor
Mechanical Engineering

_____

Dr. Alan Shihadeh, Professor   Member of Committee
Mechanical Engineering

_____

Dr. Najat Saliba, Professor   Member of Committee
Chemistry

Date of thesis/dissertation defense: December 17, 2018

AMERICAN UNIVERSITY OF BEIRUT

THESIS, DISSERTATION, PROJECT RELEASE FORM

Student Name: __Ghadban__   __Mohamad__   __Kheir__
                    Last   First   Middle

☑ Master's Thesis   ○ Master's Project   ○ Doctoral Dissertation

☑ I authorize the American University of Beirut to: (a) reproduce hard or electronic copies of my thesis, dissertation, or project; (b) include such copies in the archives and digital repositories of the University; and (c) make freely available such copies to third parties for research or educational purposes.

☐ I authorize the American University of Beirut, to: (a) reproduce hard or electronic copies of it; (b) include such copies in the archives and digital repositories of the University; and (c) make freely available such copies to third parties for research or educational purposes
after : **One ---- year from the date of submission of my thesis, dissertation, or project.**
Two ---- years from the date of submission of my thesis, dissertation, or project.
Three ---- years from the date of submission of my thesis, dissertation, or project.

Mohamad   21/12/2018
Signature   Date

This form is signed when submitting the thesis, dissertation, or project to the University Libraries

ACKNOWLEDGEMENTS

AN ABSTRACT OF THE THESIS OF

Mohamad Kheir Ghadban   for   Master of Engineering
                                      Major: Mechanical Engineering

Title: Towards Improving Weather Forecasts For Beirut Using the Coupled WRF-UCM

The coupling between the urban climate and pollution in cities has been studied extensively in the literature. In an effort to build a future pollution forecasting tool for Beirut city, obtaining meteorological variables that are representative of the city is a fundamental part.

The objective of this work was to couple a single – layer urban canopy model (UCM) with the Weather Research and Forecasting model (WRF) and to fine – tune urban parameters that are relevant to Beirut city to get weather forecasts, represented by temperature, that would represent actual weather conditions in the city. Urban parameters that were tuned included the roof albedo, wall albedo, roof thermal conductivity, wall thermal conductivity, in addition to the anthropogenic heat. To get optimum values for these parameters, simulations with different values for each parameter were performed during the four seasons and compared with observations from stations that are distributed across the city. To evaluate results and determine optimum values, different statistical parameters were used such as the mean, standard deviation, mean bias, root mean square error, and correlation coefficient.

The second part involved downscaling the velocity field obtained from WRF from the scale of 1 kilometer (WRF scale) to the scale of 1 meter while using mass conservation as a constraint and accounting for buildings and topography as no-flow-through boundaries.

CONTENTS

Chapter

I. INTRODUCTION

ILLUSTRATIONS

TABLES

ABBREVIATIONS

WRF: Weather Research and Forecasting model

EDL: Electricité du Liban

PPAH: Polycyclic Aromatic Hydrocarbons

NCAR: National Center for Atmospheric Research

NOAA: National Oceanic and Atmospheric Administration

AFWA: Air Force Weather Agency

FAA: Federal Aviation Administration

UCM: Urban Canopy Model

AH: Anthropogenic Heat

BEP: Building Effect Parametrization

USGS: United States Geological Survey

MODIS: Moderate Resolution Imaging SpectroRadiometer

IGBP: International Geosphere Biosphere Programme

NLCD: National Land Cover Database

GFS: Global Forecasting System

NCEP: National Centers for Environmental Prediction

UTC: Coordinated Universal Time

STD: Standard Deviation

MB: Mean Bias

RMSE: Root Mean Square Error

CC: Correlation Coefficient

NRMSE: Normalized Root Mean Square Error

UTM: Universal Transverse Mercator

FEM: Finite Element Method

CV: Calorific Value

رب زدني علما

CHAPTER I

INTRODUCTION

A. General Introduction

Beirut, which is the capital of Lebanon, is a coastal city that lies on the eastern shore of the Mediterranean Sea. Beirut city (the governorate) spans an area of about 18 km^2 and sits atop of two hills, Al-Achrafieh (East Beirut) and Al-Msaitbeh (West Beirut)[1].

The city has witnessed a rapid urbanization phenomenon during the past few years. One of the main causes of this phenomenon was the civil war which led to a catastrophic destruction of many buildings in Beirut. Consequently, a massive construction movement started after the war has ended. Another reason for the rapid urban expansion in Beirut is the fact that economic levels in Beirut in terms of availability of jobs and salaries are generally better than those in other regions in Lebanon. Therefore, people from rural areas tend to move to Beirut for the sake of having a better living. As a matter of fact, according to UN-Habitat [2], 88 % of Lebanon's population lived in urban areas in 2014. With the need for proper accommodation, the previous figure clearly reflects the general urban status in Lebanon and particularly in its capital Beirut.

Although urbanization might have positive effects on the urban economy, it definitely has negative ones at least on health and the environment. The need for electricity, for example, which is a fundamental source of energy is a major cause of these negative effects due to the different types and amounts of pollutants that get emitted through its generation. In general, electricity is generated for 24 hours through state – owned power

plants that are usually located in regions far from residential areas; however, in Lebanon and especially in Beirut, electricity is generated through privately owned diesel generators during outage hours i.e. during hours when there is no electricity supplied by state owned electricity suppliers, such as Electricité du Liban (EDL), due to fuel shortages. Pollutants contained in the exhaust of these generators which are usually located between buildings or on the roofs were shown to lead to additional daily exposure to airborne carcinogens such as Particle-bound Polycyclic Aromatic Hydrocarbons (PPAH) by about 65% for an outage period of 3 hours in Hamra, which is a dense urban area located in Beirut [3]. In addition to that, heavy traffic in the city with lax governmental regulations that control pollutant emissions from the car fleet add to the culprit of air pollution. Additionally, the garbage problem in the capital which is going to be disposed of by implementing incinerators is expected to exacerbate the problem. All this represents a motivation for studying the behavior and dynamics of pollutants, which are mainly controlled by meteorological variables such as the temperature and wind, in an urban area such as Beirut. One of the means of getting such meteorological variables is by using numerical weather prediction models that solve different mathematical equations based on some given initial and boundary conditions. However, to provide representative variables for the area under study, these models need to be calibrated.

B. Literature Review

Air quality models require meteorological inputs as one of the primary inputs for them to be able to simulate the dispersion of pollutants. This close coupling between meteorology and pollution dispersion has led to the development of state-of-the-art meteorological models which are shown to represent, to a large degree, actual atmospheric

2

conditions. In addition, one of the fundamental steps for air quality models after obtaining the meteorological fields is to downscale meteorological variables and other variables to a finer resolution at which the solution is desired. In what follows, an overview of the meteorological model used in this work will be presented. Additionally, the mathematical basis of the downscaling procedure will be highlighted.

1. WRF

The Weather Research and Forecasting model (WRF)[4] is a nonhydrostatic, compressible model that uses a mass coordinate system. It is the next generation open-source mesoscale numerical weather prediction tool designed for both atmospheric research and operational forecasting applications and developed by collaborative efforts of the American institutions: National Center for Atmospheric Research (NCAR), the National Oceanic and Atmospheric Administration (NOAA), the Air Force Weather Agency (AFWA), the Naval Research Laboratory, the University of Oklahoma, and the Federal Aviation Administration (FAA). It can produce simulations based on actual atmospheric conditions or idealized conditions with high accuracy[5, 6]. Also, it reflects the most recent advances in physics and numerics contributed by developers from the wide research community which consists of a total of 39,000 registered users from more than 160 countries [7], and it has a myriad of options for physical processes, land surface models, cumulus, and planetary boundary layer parametrizations.

a. <u>Urban Canopy Models</u>

To better represent physical processes involved in an urban environment such as the exchange of heat, momentum, and water vapor, urban canopy models were developed. These models, together with land surface models, when coupled with numerical weather prediction models, provide lower boundary conditions for the latter in order to get more representative weather forecasts for urban regions. The following represents some urban canopy models that are commonly used.

i. <u>Slab Model</u>

This model uses bulk urban parametrization to represent zero order effects of urban surfaces. It was initially embedded in WRF within the Noah land surface model with the following parameters being used [8]:

- roughness length of 0.8 m to represent drag caused by urban surfaces

- surface albedo of 0.15 to reflect short wave radiation trapping

- high volumetric heat capacity of 3.0 J m^{-3} K^{-1} and high soil thermal conductivity of 3.24 W m^{-1} K^{-1} to reflect heat storage from building walls

- reduced vegetation fraction to reduce evaporation

However, although it differentiates between urban and non – urban surfaces through the parameters above, it treats both building walls and the road as one surface assuming they have the same surface temperature [9].

ii. Single Layer Urban Canopy Model

This model which will be referred to hereafter as "UCM" was created to represent energy and momentum exchange between urban surfaces and the atmosphere with more realistic geometry than the slab model. It accounts for the 2D nature of street canyons, shadowing from buildings and radiation trapping. Some of the calculated variables include the surface temperatures and heat fluxes from the wall, roof, and ground [9]. One of its distinguishing features is that it accounts for anthropogenic heating (AH) through a parameter that is explicitly defined by the user and that has been proven to be a salient parameter [10, 11].

iii. Multi-Layer Urban Canopy Model

This is also called BEP [12] for building effect parametrization which also accounts for solar reflection and radiation trapping between buildings. Moreover, it recognizes the fact that buildings vertically distribute heat, momentum, and moisture through the whole urban canopy. However, unlike the UCM where buildings are embedded within the model's first vertical layer, those in BEP extend beyond the first level [13]. Furthermore, BEP acknowledges the 3D nature of buildings and doesn't allow for an explicit specification of AH but accounts for it implicitly. A major drawback of this sophisticated model is that it requires high vertical resolution in the vicinity of the ground which is only attainable when computational resources are not a constraint [10, 13]. The figure below illustrates the difference between UCM and BEP.
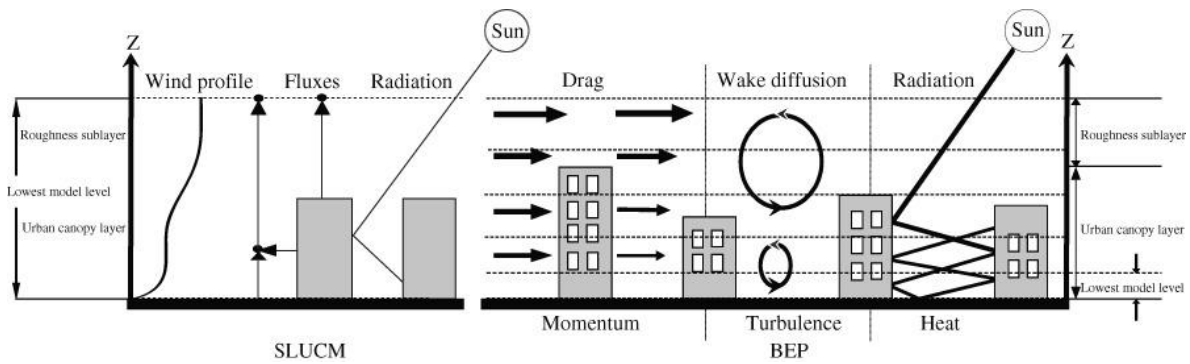
Figure 1: Comparison of UCM and BEP (from [13])

2. Downscaling

As stated earlier, wind plays an essential role in the dynamics and dispersion of air pollutants because it acts as a driver to air contaminants. However, the scale at which the wind field is represented is of great importance. For example, when studying pollution dispersion at the pedestrian level which is at the scale of few meters, a wind field that is represented at the scale of kilometers will not be representative of actual pollutants behavior. This necessitates the need for downscaling the velocity field, while conserving physical laws, to that of the pedestrian scale to obtain results that are more representative. Mesoscale numerical weather prediction models including WRF usually produce wind fields on grid points with a resolution of few kilometers. Moreover, meteorological observational stations aren't usually located at the desired spatial resolution if their wind data is to be used. This proves the momentousness of downscaling.

A myriad of downscaling models have been developed and they generally fall into two categories: "**prognostic**" or "dynamic" and "**diagnostic**" models [14]. Although they're both meant to simulate wind fields over a terrain, prognostic models solve the time dependent

hydrodynamic and thermodynamic equations and account for numerous physical phenomena such as advection, Coriolis force, and radiation to name a few. However, the solution to these equations is usually taxing and is computationally expensive. On the other hand, diagnostic models are time independent meaning that forecasting in time is not possible as explained by Pielke [15]. These models also generate wind fields based on satisfying physical constraints. When these models use mass conservation as the physical constraint, they are called mass – consistent models which are based on the steady state three – dimensional continuity or mass conservation equation. The simplicity of these models and their ability to generate a 3D mass consistent wind field with only few inputs in addition to being computationally economical is what made them attractive for downscaling the velocity field. The downscaling procedure generally involves two steps [14]:

- initializing the velocity field at all grid points of the domain through interpolation/extrapolation of available data, hereafter referred to as "observations", which could be from observational weather stations or numerical weather prediction models
- minimizing the divergence of the interpolated/extrapolated velocity field using an adjustment procedure

According to Ratto et al. [14], the horizontal interpolation/extrapolation scheme that is commonly used is the $1/r^2$ law where r is the distance between each grid point and the point at which observational data exist. As for vertical interpolation, the power law

$$V = V_0 \left(\frac{z}{z_0}\right)^p$$

is the one that is widely used where "V" is the extrapolated velocity component at height "z", "V_0" is the observed velocity component at height "z_0", and "p" has the value of approximately 1/7 based on neutral atmospheric conditions [16, 17].

As for the second step of the downscaling procedure, different methods were developed to minimize the divergence of the interpolated velocity field. Of these methods, "direct differencing" and "variational calculus" are the most frequently used [17]. The first method solves the continuity equation numerically where the horizontal velocity field (u and v) is numerically differentiated at each grid point so that the vertical velocity (w) can be obtained after initializing it to zero at the topography [18-20]. On the other hand, the variational calculus method which was developed by Sasaki [21, 22] aims to minimize the variance of the difference between an observed/interpolated variable and the analyzed variable, which is the adjusted velocity field in our case, by defining an integral function whose solution is subject to "strong" physical constraints that have to be satisfied exactly by the analyzed variable, or to "weak" constraints that have to be satisfied approximately by the same variable. The continuity equation; however, is the most frequently used as a strong constraint to adjust the interpolated velocity field because it ensures that transported mass across a domain is conserved as in [16, 17, 23-25]. Although additional physical constraints can be used such as preserving the observed vorticity field as was done by Mathur and Peters [24], the authors concluded that the inclusion of the vorticity as a constraint is not critical and that considering mass conservation as the only constraint would result in an adjusted velocity field that is representative of realistic fields and consistent with general physical relations.

In addition, Kitada et al. [17], in their study, performed a comparison between the direct differencing technique and the variational calculus one. They found out that although both methods produce adjusted wind fields of the same pattern, direct differencing requires very accurate horizontal wind field as input; otherwise, resultant vertical wind velocities will be unreasonable proving the powerful capabilities of the variational calculus method which were also stressed by Mathur and Peters [24].

As stated earlier, the variational calculus method aims to minimize the variance between the interpolated velocity field and the adjusted velocity field while satisfying mass conservation as a strong constraint which can be mathematically expressed as [16]:

$$J(x, y, z, \lambda) = \int_{\Omega} (\alpha_1(u - u^0)^2 + \alpha_2(v - v^0)^2 + \alpha_3(w - w^0)^2 + \lambda G)dV \qquad (1)$$

where $u^0, v^0, and\ w^0$ are the interpolated velocity components

$u, v, and\ w$ are the adjusted velocity components

$$G = \frac{\partial u}{\partial x} + \frac{\partial v}{\partial y} + \frac{\partial w}{\partial z} \qquad (2)$$

λ is the lagrange multiplier

Ω is the domain of study

In the equation above, $\alpha_1, \alpha_2, and\ \alpha_3$ represent the amount of adjustment applied to the horizontal (u and v) and vertical (w) velocity components. However, it was found in the literature that $\alpha_1 and\ \alpha_2$ were always assumed to be identical i.e. $\alpha_1 = \alpha_2$ while α_3 can be identical or different [14]. The Euler-Lagrange equations whose solution minimizes the above equation are:

9

$$u = u^0 + \frac{1}{2\alpha_1^2}\left(\frac{\partial\lambda}{\partial x}\right) \tag{3}$$

$$v = v^0 + \frac{1}{2\alpha_2^2}\left(\frac{\partial\lambda}{\partial y}\right) \tag{4}$$

$$w = w^0 + \frac{1}{2\alpha_3^2}\left(\frac{\partial\lambda}{\partial z}\right) \tag{5}$$

By substituting equations (3), (4), and (5) in the continuity equation, the following form will be obtained [16]:

$$\frac{\partial^2\lambda}{\partial x^2} + \frac{\partial^2\lambda}{\partial y^2} + \left(\frac{\alpha_1}{\alpha_3}\right)^2\frac{\partial^2\lambda}{\partial z^2} = -2\alpha_1^2\left(\frac{\partial u^0}{\partial x} + \frac{\partial v^0}{\partial y} + \frac{\partial w^0}{\partial z}\right) \tag{6}$$

with the following boundary conditions:

1) $\lambda = 0$ on an open boundary implying a non – zero adjustment to the velocity component normal to that boundary i.e. only the normal velocity component is adjusted.

2) $\frac{\partial\lambda}{\partial n} = 0$ on a closed boundary such as the topography where "n" is the outward positive unit vector normal to the closed boundary. This boundary condition results in adjustment to the velocity components that are parallel to the closed boundary and zero adjustment to the normal velocity component as can be seen in equations (3), (4), and (5). Hence the second part of this project aimed at solving Eq. (6) for λ, consequently calculating the adjusted velocity field. Furthermore, different values for the ratio $\left(\frac{\alpha_1}{\alpha_3}\right)^2$ were considered to determine an optimum value that would result in a flow field with minimum total residual divergence.

C. Research Statement

The primary objective of this research project was to answer the following question: can we get better forecasts for Beirut city that would be representative of actual weather conditions represented by temperature? To answer this question, the urban canopy model UCM was coupled with WRF and urban parameters were tuned to reflect the urban status in the city of Beirut as much as possible. The advantage of this tuning process is two-fold, the first is getting a weather forecast for Beirut that represents – as much as possible – actual weather conditions in the city, and the second is obtaining a velocity field that can be used as input for future pollution transport models.

The other part of this research involved an "initial effort" in downscaling the velocity field obtained from WRF from the scale of 1 kilometer (WRF scale) to the scale of 1 meter (pedestrian scale) while respecting one of the fundamental physical laws which is mass conservation in addition to accounting for buildings and topography as no – flow – through boundaries. This high – resolution downscaled wind field which is at the pedestrian level would serve as an input to future pollution dispersion models aimed to study pollution dynamics in Beirut at high resolutions.

CHAPTER II

METHODOLOGY

In this chapter, the methodology that was adopted for the tuning process will be discussed in which the domain setup, the initialization procedure, the actual calibration process, observational data, and model evaluation will be examined in detail. Furthermore, the discretization of equation (6) using the Finite Element Method will be discussed.

A. WRF – UCM Tuning

1. Domain Setup

For this study, a parent domain (D1) and two nested domains (D2 and D3) were used. The largest domain D1 covered part of the Mediterranean area while the remaining smaller domains D2 and D3 covered Lebanon and Beirut respectively as can be seen in Figure 2. As for dimensions, 100x100, 61x73, and 40x40 grid points in the west-east and south-north directions were used to represent domains D1, D2, and D3 respectively with corresponding spatial resolutions of 9 km, 3 km, and 1 km in the x and y directions.

With regards to land use which is an essential part in urban modelling, WRF has three main land use datasets to interpolate from: 1) the United States Geological Survey (USGS), 2) Moderate Resolution Imaging SpectroRadiometer (MODIS) International Geosphere Biosphere Programme (IGBP), and 3) National Land Cover Database (NLCD). While the third dataset only covers locations in the U.S., the first two are global but differ in spatial resolutions where the resolution of USGS data is 30 arc-seconds ($\sim 900\ m$) unlike

that of MODIS IGBP which is 15 arc-seconds ($\sim 450\ m$). Hence, the latter was chosen for land use data.
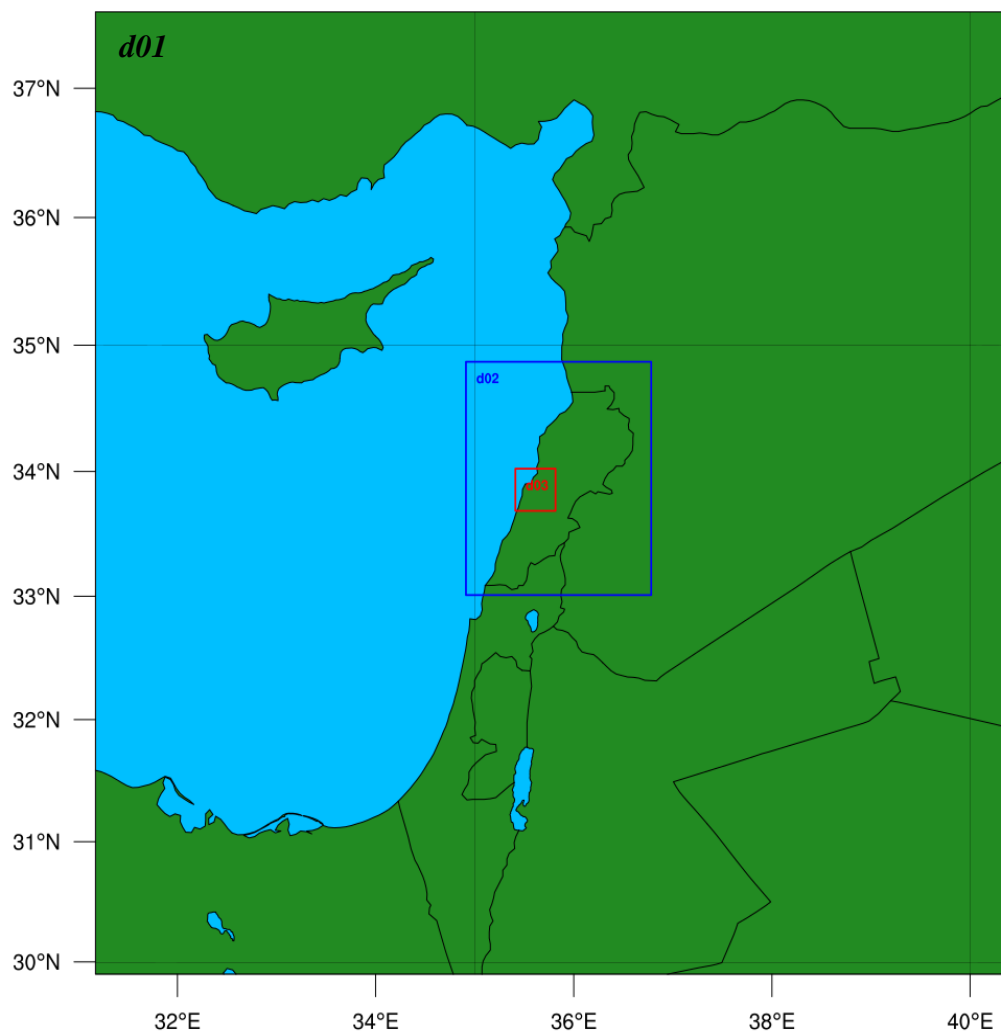
Figure 2: Domains used in WRF with "d03" with a red border representing Beirut, the area under study.

2. Initialization and Boundary Conditions

WRF requires initial and lateral meteorological boundary conditions as input to be able to produce a forecast or to run a simulation (hindcast). For this purpose, data from the Global Forecast System (GFS) which is a weather model run by the National Centers for Environmental Prediction (NCEP) was used. This model uses the maximum amount of satellite measurements and global observations and runs four times per day at 0000, 0600, 1200, and 1800 UTC to produce forecasts for the following 16 days. These forecasts are used as initial and boundary conditions to run WRF. Knowing that the GFS model produces data at different spatial resolutions (0.25, 0.5, and 1.0 degrees), the finest resolution of 0.25 degrees, which was recently introduced, was used. This data was obtained from the Research Data Archive [26].

3. UCM Calibration

WRF comes with an option called "sf_urban_physics" which when set to "0" means that UCM will not be incorporated and when set to "1" indicates that UCM will be used along with all its parametrizations. In addition to activating UCM, urban parameters pertinent to the urban area need to be adjusted accordingly. These urban parameters form a long list consolidated in a table called "URBPARM.TBL" which is an editable text file. Some of these parameters are geometrical such as the average height of buildings, average roof width, and average road width and some are related to the thermal characteristics of the urban environment such as the anthropogenic heat (AH), average surface albedo of buildings' roofs and walls, their average thermal conductivity and heat capacity, in addition to many other parameters.

In the table previously mentioned, there are three columns corresponding to different levels of urbanization, namely low intensity residential, high intensity residential, and commercial/industrial. The first type corresponds to urban areas with a mixture of constructed areas and vegetation with the majority of people residing in single-family houses. The second category corresponds to highly populated urban areas where vegetation accounts for less than 20 % of the land cover while constructed areas account for 80 to 100 % of the cover. The third category corresponds to urban areas that are not considered as one of the first two classifications [27]. Beirut was considered as a high intensity residential area by WRF-UCM since changing parameters corresponding to the other two urban categories did not result in any changes in simulated meteorological variables.

Having determined the urban classification of Beirut and consequently the column to modify, parameters, namely the average height of buildings and its standard deviation, roof albedo, wall albedo, AH, roof thermal conductivity, and wall thermal conductivity were calculated/tuned (see Table 1) to reflect representative values of Beirut. Of these parameters, the average buildings height and its standard deviation were set based on a shapefile for Beirut which contains the heights of all buildings in the city, so simple arithmetic mean and standard deviation calculations were performed to get the corresponding values. In addition, the value of the wall's thermal conductivity was calculated assuming the wall is made up of three layers: a concrete block (10 cm thick) that is sandwiched between two stucco layers (2.5 cm thick each) on both sides. Consequently, the following formula was used:

$$k_{wall} = \frac{l_{total}}{R_{total}} \; where \; l_{total} \; is \; the \; total \; thicknes \; of \; the \; wall \qquad (7)$$

$$and\ R_{total}{}^{1}\ is\ the\ total\ thermal\ resistance\ of\ the\ wall$$

$$\Rightarrow k_{wall} = \frac{2x0.025 + 0.1}{2x0.03519 + 0.08} = 0.997 \frac{W}{m.^{0}\,K}$$

Since no representative values exist for the rest of the selected parameters for Beirut [28], they were tuned by changing one parameter at a time and then choosing the optimum value at which simulated temperature and wind speed closely matched observed values (refer to section 5).

Table 1: UCM parameters that were tuned or calculated

PARAMETER	CALCULATED/TUNED	CALCULATED VALUE
ROOF HEIGHT	calculated	19 m
STD OF ROOF HEIGHT	calculated	12.9 m
ROOF ALBEDO	tuned	-
WALL ALBEDO	tuned	-
AH	tuned	-
ROOF THERMAL CONDUCTIVITY	tuned	-
WALL THERMAL CONDUCTIVITY	calculated	0.997 W/m.^{0}k

4. Observational Data

Three different stations located in Beirut were chosen with which simulated temperatures and wind speeds were compared. The three stations – hereafter designated as "Stn1", "Stn2", and "Stn3" – are located in *Achrafieh*, *Baabda*, and *The American University*

---

[1] Individual resistances of materials were taken from Carrier's Hourly Analysis Program (HAP)

of Beirut (*Elmer and Mamdouha Bobst Chemistry Building*) respectively (Figure 3) with their coordinates being shown in Table 2.

Figure 3: Location of stations from which observed temperatures and wind speed were extracted

Table 2: Latitude, Longitude, and Elevation of the three stations

Station	Lat	Lon	Elevation[2]
Stn1	33.885	35.51639	103 m
Stn2	33.85111111	35.53805556	110 m
Stn3	33.901024	35.479201	40 m

---

[2] Elevation is above sea level

These stations, except for Stn3, are hooked up with a renowned weather data repository called "Weather Underground" which collects data from more than 250,000 weather stations from around the world. This repository, in addition to offering free weather data at different temporal resolutions (daily, weekly, monthly, and yearly), it performs perennial quality control checks through algorithms specifically built by data scientists to ensure that the best data is reported [29]. Hence, data from the first two stations was collected from this repository for the whole period of study while data from the third station was collected from the *Chemistry Building*.

5. Study Period and Model Evaluation

To ensure the representativeness of the tuned parameters, simulations were performed for 8 days in each of the four seasons. During the summer, fall, winter, and spring seasons of the year 2017, simulations were performed from July 20 to 27, October 20 to 27, January 20 to 27, and April 20 to 27 respectively. The choice of the time period was based on the representativeness of observed weather data to average weather conditions during each season and on the availability of observed data. In addition, it is noteworthy that the first 24 hours of each simulation were considered as a spin up period and consequently were left out of the analysis. Therefore, simulated data from the 21st to the 27th of each month were effectively used in the statistical analysis.

As previously mentioned (in section 3), after each change in the value of a parameter, simulated temperature and wind speed were compared with observed values. Since the spatial resolution of D3 is 1 km, values at each grid point are not representative of sub – grid values; thus, to get simulated values at the exact location of a station, a bilinear

18

interpolation was performed in the horizontal direction and a linear interpolation in the vertical direction. Different statistical parameters were used such as the Mean, Standard Deviation (STD), Mean Bias (MB), Root Mean Square Error (RMSE) and Correlation Coefficient (CC) where the RMSE was the major parameter in determining optimum values of tuned parameters. For each parameter to be tuned, and after running multiple simulations with different values for that parameter, the mean of each statistical parameter was calculated for each simulation and for all stations. However, during the month of July, the number of observations at Stn3 (107) was less than that at the other two stations (165), so the ratio between the number of observations at Stn1 and that at Stn3 was used to calculate the weighted-mean in lieu of the arithmetic mean when averaged values for all stations were calculated. This averaging process was performed for both the temperature and the wind speed; hence, resulting in two sets of data, one for the temperature and the other for the wind speed, which represent average values at all stations. However, since the objective was to get optimum parameters that would correspond to simulated temperature and wind speeds that are as close as possible to observations, a weighted average of the RMSE between the two data sets was needed. But since the scales of the temperature and wind speed are different, the RMSE was normalized by the mean and resulted in the Normalized RMSE (NRMSE) so that the averaging process can be done on a one to one basis. Having calculated the NRMSE for each data set, the weighted mean of this parameter was calculated by using the CC's as weights. After having a single value for the NRMSE for both meteorological variables, the optimum value of the tuned parameter which corresponds to the minimum NRMSE was selected. This optimum value was then set in URBPARM.TBL and tuning of the other

```
                    ┌──────────────────────┐
                    │  Select parameter to be │
                    │        tuned            │
                    └──────────────────────┘
                              │
                    ┌──────────────────────┐
                    │  Run simulations using │
                    │  different values for this │
                    │        parameter        │
                    └──────────────────────┘
                              │
                    ┌──────────────────────┐
                    │ Extract data at all stations │
                    └──────────────────────┘
```

Select parameter to be tuned

Run simulations using different values for this parameter

Extract data at all stations

Temperature

Wind speed

Calculate the weighted average of each simulation for all stations

Calculate the weighted average of each simulation for all stations

Calculate NRMSE for each simulation

Calculate NRMSE for each simulation

Calculate the weighted average of both NRMSE values

Find min (NRMS) and select the corresponding value of the tuned parameter

Set this value in URBPARM.TBL

Figure 4: Flow chart describing the methodology used in the tuning process

parameters followed in a similar way. The flow chart above summarizes the steps previously mentioned.

It is noteworthy that optimum values of the physical parameters such as the roof albedo, wall albedo, and thermal conductivity of the roof were obtained based on the simulations performed during the months of July and October only because of two reasons the first of which is that these parameters are considered constant because they reflect materials' properties and the second is that data from Stn3 was available during these months only, for the days considered in this study. Therefore, optimum values obtained for these parameters based on statistical analysis for these months were used during the simulations in the remaining months of January and April to get corresponding optimum values for AH.

B. Downscaling the Velocity Field

1. Digitizing Buildings and Topography

To be able to downscale the velocity from WRF's scale (1 km) to the scale of 1 m, a 3D structured computational grid was needed on which computations were performed. In addition to that, boundaries deemed necessary for the downscaling algorithm such as buildings and topography needed to be digitized and numerically represented. As such, buildings in Beirut, which were obtained from an urban planner and contained in a shapefile (.shp), were extracted using ArcGIS which is a geographic information system software. This shapefile contained about 18500 buildings as well as values of the geographic coordinates of the vertices of each building (longitude and latitude) in addition to the buildings' heights. Since these buildings needed to be represented on a cartesian grid, the "lat/lon" coordinates were transformed into the Universal Transverse Mercator (UTM) coordinates using the same

21

software. After transforming coordinates, data from this shapefile was then written to a text file which was read using FORTRAN to store the information of buildings in arrays.

Since it would be very computationally expensive to downscale the velocity field at all grid points representing the city, a simplified domain was sought. For this purpose, a small area near *Al Msaytbeh* was selected with dimensions 50 x 50 m^2 in the x and y directions. Consequently, a computational grid with 50 nodes in the x direction, 50 nodes in the y direction and 12 nodes in the z direction was built with a resolution of 1 m in all three directions. Having the computational grid built, only buildings located in this area as well as topography points representing this area were used in the downscaling model.

Before moving on to the downscaling procedure, projecting buildings and topography onto the computational grid was necessary because the FEM seeks to find a solution at each grid point or node and because boundary conditions are imposed on these nodes as well. Hence, to project each building, the base was only considered and then the top of the building was simply an extrusion of the base. Subsequently, the side of each base was divided into very small and equidistant points using isoparametric mapping where each point in the natural or intrinsic coordinate system was mapped to the Cartesian coordinate system using special interpolation functions (see Figure 5) which are also called shape functions [30]. Each point along the edge was then projected onto the nearest neighboring node. Having the base projected, the nodes at the top of the building were easily constructed using the height of each building.

With regards to the topography, it was digitized and projected onto the grid by a member of the research group using Google Sketchup and Rhinoceros where it was represented by points with coordinates (x and y) in UTM coordinate system, elevation (z)

22

above sea level, and a resolution of 1 m meaning that the distance between any two adjacent points is 1 m. Attributes of these points were also written to a text file and read by the FORTRAN code.
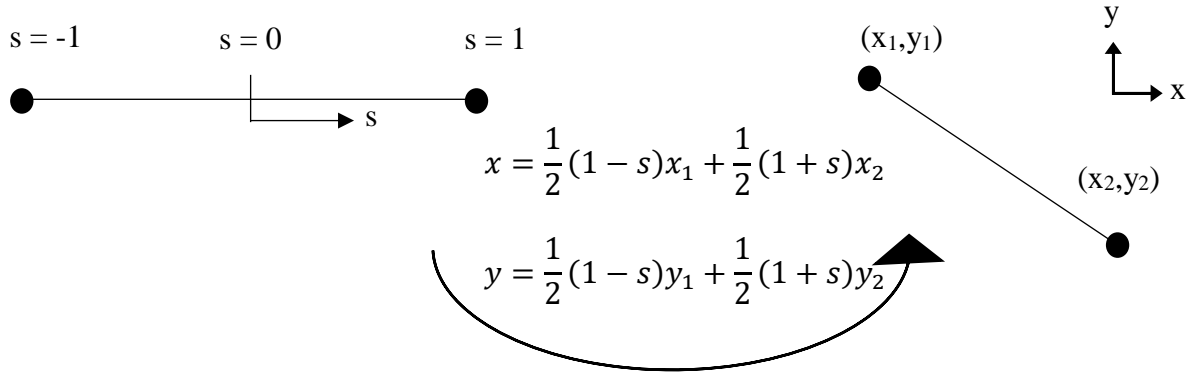
Figure 5: Mapping between the natural and the Cartesian coordinate systems

2. Computational Formulation: The Finite Element Method

As mentioned earlier, the objective was to solve the equation for "λ" and then plug it in the corresponding equations of u, v, and w to adjust the velocity components and calculate the new divergence. However, this equation has the shape of what is referred to in the literature as "Poisson's Equation" which is of the form:

$$k_x \frac{\partial^2 \lambda}{\partial x^2} + k_y \frac{\partial^2 \lambda}{\partial y^2} + k_z \frac{\partial^2 \lambda}{\partial z^2} = -Q(x, y, z) \tag{8}$$

If we do a short comparison with the equation to be solved, we notice that:

$$k_x = k_y = 1$$

$$k_z = \left(\frac{\alpha_1}{\alpha_3}\right)^2$$

$$Q = 2\alpha_1^2 \left(\frac{\partial u^0}{\partial x} + \frac{\partial v^0}{\partial y} + \frac{\partial w^0}{\partial z}\right) = 2\alpha_1^2 \nabla.\overrightarrow{V^0}$$

23

where u^0, v^0, and w^0 are the interpolated velocity components to be adjusted.

The discretization procedure of (8) yields the following set of equations:

$$[K]\{\lambda\} = \{Q\} \tag{9}$$

which is analogous to $[A]\{x\} = \{b\}$

a. <u>Assembly of the System of Equations: $[\boldsymbol{K}]\{\boldsymbol{\lambda}\} = \{\boldsymbol{Q}\}$</u>

To assemble the above equations, the following steps were taken as in [30]

i. <u>Select Element Type</u>

Since the problem is 3D, a *linear hexahedral element* which is also called a *brick element* was considered with the node numbering as shown below.
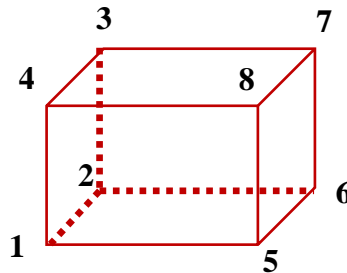
ii. <u>Select a Profile for λ</u>

Since the element chosen is three dimensional, the analysis was performed using isoparametric formulation where equations are written in terms of the natural coordinates s, t, and z' instead of x, y, and z which will make volume integration much easier as will be seen later.
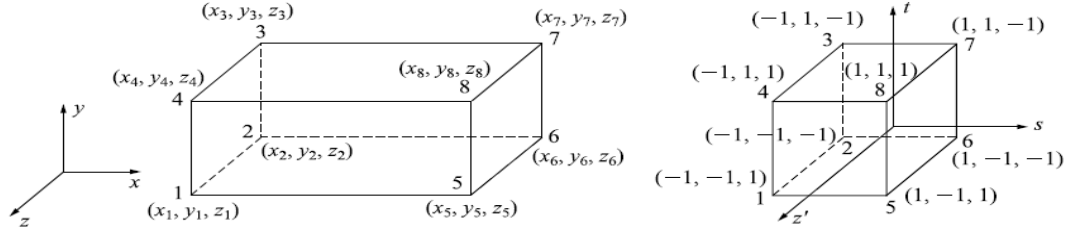
Figure 6: Nodal global and natural coordinates

Having said that, a linear profile was selected for the mapping process of the linear brick element:

$$x = a_1 + a_2 s + a_3 t + a_4 z' + a_5 st + a_6 tz' + a_7 z's + a_8 stz' \tag{10}$$

$$y = a_9 + a_{10}s + a_{11}t + a_{12}z' + a_{13}st + a_{14}tz' + a_{15}z's + a_{16}stz' \tag{11}$$

$$z = a_{17} + a_{18}s + a_{19}t + a_{20}z' + a_{21}st + a_{22}tz' + a_{23}z's + \tag{12}$$

$$a_{24}stz'$$

After substituting for each node its corresponding coordinates, the 'a's can be determined. For example, if we substitute the coordinates of node "i" in the equation of "x" where i: 1 → 8, we can determine the unknows a1 → a8 i.e.

$$x_i = a_1 + a_2 s_i + a_3 t_i + a_4 z'_i + a_5 s_i t_i + a_6 t_i z'_i + a_7 z'_i s_i + a_8 s_i t_i z'_i \tag{13}$$

The other unknowns i.e. a_9 → a_{24} can be determined by doing similar substitutions in the equations of "y" and "z". After determining the unknows, the previous equations were rearranged in the form of:

$$\{x\} = [N]\{d\} \, where \, \{d\} = x_1 \rightarrow x_8 \tag{14}$$

$$\{y\} = [N]\{d\} \, where \, \{d\} = y_1 \rightarrow y_8 \tag{15}$$

$$\{z\} = [N]\{d\} \, where \, \{d\} = z_1 \rightarrow z_8 \tag{16}$$

where the shape functions [N] - which is a 1x8 - vector were determined. The general form

of the shape functions is: $N_i = \frac{(1+ss_i)(1+tt_i)(1+z'z_i')}{8}$ $where\ i: 1 \rightarrow 8$ which implies that the

shape function at each node is:

$$N_1 = \frac{(1-s)(1-t)(1+z')}{8} \qquad\qquad N_5 = \frac{(1+s)(1-t)(1+z')}{8}$$

$$N_2 = \frac{(1-s)(1-t)(1-z')}{8} \qquad\qquad N_6 = \frac{(1+s)(1-t)(1-z')}{8} \qquad (17)$$

$$N_3 = \frac{(1-s)(1+t)(1-z')}{8} \qquad\qquad N_7 = \frac{(1+s)(1+t)(1-z')}{8}$$

$$N_4 = \frac{(1-s)(1+t)(1+z')}{8} \qquad\qquad N_8 = \frac{(1+s)(1+t)(1+z')}{8}$$

iii. Get the Gradient of "λ"

Having found the shape functions, the gradient of "λ", which is defined below, was

determined:

$$\{\nabla\lambda\} = [B]\{d\} \qquad\qquad (18)$$

$$where\ \{\nabla\lambda\} = \begin{Bmatrix} \frac{\partial\lambda}{\partial x} \\ \frac{\partial\lambda}{\partial y} \\ \frac{\partial\lambda}{\partial z} \end{Bmatrix} \qquad\qquad (19)$$

$$[B] = \begin{bmatrix} \frac{\partial N}{\partial x} \\ \frac{\partial N}{\partial y} \\ \frac{\partial N}{\partial z} \end{bmatrix} \qquad\qquad (20)$$

$$\text{and } \{d\} = \begin{Bmatrix} d_1 \\ \vdots \\ d_8 \end{Bmatrix} \text{ which is an 8x1 vector} \tag{21}$$

However, since λ is a function of s, t, and z', the Jacobian matrix [J] was needed

since

$$\frac{\partial \lambda}{\partial x} = \frac{1}{|J|} \begin{vmatrix} \dfrac{\partial \lambda}{\partial s} & \dfrac{\partial y}{\partial s} & \dfrac{\partial z}{\partial s} \\ \dfrac{\partial \lambda}{\partial t} & \dfrac{\partial y}{\partial t} & \dfrac{\partial z}{\partial t} \\ \dfrac{\partial \lambda}{\partial z'} & \dfrac{\partial y}{\partial z'} & \dfrac{\partial z}{\partial z'} \end{vmatrix} \;;\; \frac{\partial \lambda}{\partial y} = \frac{1}{|J|} \begin{vmatrix} \dfrac{\partial x}{\partial s} & \dfrac{\partial \lambda}{\partial s} & \dfrac{\partial z}{\partial s} \\ \dfrac{\partial x}{\partial t} & \dfrac{\partial \lambda}{\partial t} & \dfrac{\partial z}{\partial t} \\ \dfrac{\partial x}{\partial z'} & \dfrac{\partial \lambda}{\partial z'} & \dfrac{\partial z}{\partial z'} \end{vmatrix} \;;\; \frac{\partial \lambda}{\partial z} = \frac{1}{|J|} \begin{vmatrix} \dfrac{\partial x}{\partial s} & \dfrac{\partial y}{\partial s} & \dfrac{\partial \lambda}{\partial s} \\ \dfrac{\partial x}{\partial t} & \dfrac{\partial y}{\partial t} & \dfrac{\partial \lambda}{\partial t} \\ \dfrac{\partial x}{\partial z'} & \dfrac{\partial y}{\partial z'} & \dfrac{\partial \lambda}{\partial z'} \end{vmatrix} \tag{22}$$

$$\text{where } [J] = \begin{bmatrix} \dfrac{\partial x}{\partial s} & \dfrac{\partial y}{\partial s} & \dfrac{\partial z}{\partial s} \\ \dfrac{\partial x}{\partial t} & \dfrac{\partial y}{\partial t} & \dfrac{\partial z}{\partial t} \\ \dfrac{\partial x}{\partial z'} & \dfrac{\partial y}{\partial z'} & \dfrac{\partial z}{\partial z'} \end{bmatrix} \text{ and} \tag{23}$$

$$|J| = \left[\frac{\partial x}{\partial s} \left(\frac{\partial y}{\partial t} \frac{\partial z}{\partial z'} - \frac{\partial z}{\partial t} \frac{\partial y}{\partial z'} \right) - \frac{\partial y}{\partial s} \left(\frac{\partial x}{\partial t} \frac{\partial z}{\partial z'} - \frac{\partial z}{\partial t} \frac{\partial x}{\partial z'} \right) + \frac{\partial z}{\partial s} \left(\frac{\partial x}{\partial t} \frac{\partial y}{\partial z'} - \frac{\partial y}{\partial t} \frac{\partial x}{\partial z'} \right) \right] \tag{24}$$

Hence, by substituting the gradients of λ in Eq. (19), we get:

$$\begin{Bmatrix} \dfrac{\partial \lambda}{\partial x} \\ \dfrac{\partial \lambda}{\partial y} \\ \dfrac{\partial \lambda}{\partial z} \end{Bmatrix} = \frac{1}{|J|} \begin{bmatrix} A_1 \dfrac{\partial \lambda}{\partial s} & - B_1 \dfrac{\partial \lambda}{\partial t} & + c1 \dfrac{\partial \lambda}{\partial z'} \\ -A_2 \dfrac{\partial \lambda}{\partial s} & + B_2 \dfrac{\partial \lambda}{\partial t} & - c2 \dfrac{\partial \lambda}{\partial z'} \\ A_3 \dfrac{\partial \lambda}{\partial s} & - B_3 \dfrac{\partial \lambda}{\partial t} & + c3 \dfrac{\partial \lambda}{\partial z'} \end{bmatrix} = \frac{1}{|J|} \begin{bmatrix} A_1 \dfrac{\partial N}{\partial s} & - B_1 \dfrac{\partial N}{\partial t} & + C_1 \dfrac{\partial N}{\partial z'} \\ -A_2 \dfrac{\partial N}{\partial s} & + B_2 \dfrac{\partial N}{\partial t} & - C_2 \dfrac{\partial N}{\partial z'} \\ A_3 \dfrac{\partial N}{\partial s} & - B_3 \dfrac{\partial N}{\partial t} & + C_3 \dfrac{\partial N}{\partial z'} \end{bmatrix} \{d\} \tag{25}$$

where

$$A_1 = \frac{\partial y}{\partial t} \frac{\partial z}{\partial z'} - \frac{\partial z}{\partial t} \frac{\partial y}{\partial z'} \qquad B_1 = \frac{\partial y}{\partial s} \frac{\partial z}{\partial z'} - \frac{\partial z}{\partial s} \frac{\partial y}{\partial z'} \qquad C_1 = \frac{\partial y}{\partial s} \frac{\partial z}{\partial t} - \frac{\partial z}{\partial s} \frac{\partial y}{\partial t}$$

$$A_2 = \frac{\partial x}{\partial t} \frac{\partial z}{\partial z'} - \frac{\partial z}{\partial t} \frac{\partial x}{\partial z'} \qquad B_2 = \frac{\partial x}{\partial s} \frac{\partial z}{\partial z'} - \frac{\partial z}{\partial s} \frac{\partial x}{\partial z'} \qquad C_2 = \frac{\partial x}{\partial s} \frac{\partial z}{\partial t} - \frac{\partial z}{\partial s} \frac{\partial x}{\partial t}$$

$$A_3 = \frac{\partial x}{\partial t}\frac{\partial y}{\partial z'} - \frac{\partial y}{\partial t}\frac{\partial x}{\partial z'} \qquad B_3 = \frac{\partial x}{\partial s}\frac{\partial y}{\partial z'} - \frac{\partial y}{\partial s}\frac{\partial x}{\partial z'} \qquad C_3 = \frac{\partial x}{\partial s}\frac{\partial y}{\partial t} - \frac{\partial y}{\partial s}\frac{\partial x}{\partial t}$$

$$[N] = [N_1 \dots N_8]$$

$$\Rightarrow \begin{Bmatrix} \frac{\partial \lambda}{\partial x} \\ \frac{\partial \lambda}{\partial y} \\ \frac{\partial \lambda}{\partial z} \end{Bmatrix} = [B_1\ B_2\ B_3\ B_4\ B_5\ B_6\ B_7\ B_8]\{d\} = [B]\{d\}$$

$$\text{where } B_i = \frac{1}{|J|} \begin{bmatrix} A_1 \frac{\partial N_i}{\partial s} & - & B_1 \frac{\partial N_i}{\partial t} & + & C_1 \frac{\partial N_i}{\partial z'} \\ -A_2 \frac{\partial N_i}{\partial s} & + & B_2 \frac{\partial N_i}{\partial t} & - & C_2 \frac{\partial N_i}{\partial z'} \\ A_3 \frac{\partial N_i}{\partial s} & - & B_3 \frac{\partial N_i}{\partial t} & + & C_3 \frac{\partial N_i}{\partial z'} \end{bmatrix} \text{ and } i: 1 \to 8 \qquad (26)$$

$$\text{and } [B] = [B_1 \dots B_8]$$

iv. <u>Obtain the Element Stiffness Matrix and Force Vector</u>

The stiffness matrix was determined by applying the volume integral below:

$$[K]_{element} = \int_V [B]^T [D][B]\, dV \qquad (27)$$

where [B] was found in the previous step and [D] is a 3x3 matrix representing the coefficients

of the left-hand side of Eq. (8):

$$[D] = \begin{bmatrix} k_x & 0 & 0 \\ 0 & k_y & 0 \\ 0 & 0 & k_z \end{bmatrix} = \begin{bmatrix} 1 & 0 & 0 \\ 0 & 1 & 0 \\ 0 & 0 & \left(\frac{\alpha_1}{\alpha_3}\right)^2 \end{bmatrix} \qquad (28)$$

However, since [B] is a function of s, t, and z' and $dV = dxdydz$, then multiplication by $|J|$ was needed so that the integration is performed with respect to the natural coordinates s, t, and z'

$$\Rightarrow [K]_{element} = \int_{-1}^{1} \int_{-1}^{1} \int_{-1}^{1} [B]^T[D][B]|J|dsdtdz' \qquad (29)$$

Having all the needed terms as a function of the natural coordinates with integration bounds between -1 and 1, the integral was easily evaluated using Gaussian quadrature where the 2x2x2 rule was used. Thus Eq. 29 became equivalent to

$$[K]_{element} = \Sigma_{i=1}^{8}[B(s_i, t_i, z'_i)]^T[D][B(s_i, t_i, z'_i)]|J(s_i, t_i, z'_i)|dsdtdz' \qquad (30)$$

where the weights of the Gaussian quadrature are equal to unity for the 2x2x2 rule. The table below shows the Gauss points that were used.

Table 3: Gauss Points for a 2x2x2 Gauss rule

Points, i	s_i	t_i	z'_i	Weight, W_i
1	$-1/\sqrt{3}$	$-1/\sqrt{3}$	$1/\sqrt{3}$	1
2	$1/\sqrt{3}$	$-1/\sqrt{3}$	$1/\sqrt{3}$	1
3	$1/\sqrt{3}$	$1/\sqrt{3}$	$1/\sqrt{3}$	1
4	$-1/\sqrt{3}$	$1/\sqrt{3}$	$1/\sqrt{3}$	1
5	$-1/\sqrt{3}$	$-1/\sqrt{3}$	$-1/\sqrt{3}$	1
6	$1/\sqrt{3}$	$-1/\sqrt{3}$	$-1/\sqrt{3}$	1
7	$1/\sqrt{3}$	$1/\sqrt{3}$	$-1/\sqrt{3}$	1
8	$-1/\sqrt{3}$	$1/\sqrt{3}$	$-1/\sqrt{3}$	1

Regarding the force vector, the right-hand side of Eq. (8), it was discretized as follows:

$$\{Q\} = \int_{V} [N]^T Q(x, y, z)dV \qquad (31)$$

Again, since $[N]^T$ is a function of the natural coordinates, multiplication by the determinant of the Jacobian matrix was needed and integration using Gaussian quadrature followed yielding:

$$Q_{element} = \sum_{i=1}^{8} (\nabla . \overrightarrow{V^0})_{element} [N(s_i, t_i, z_i')]^T \; |J(s_i, t_i, z'_i)| \qquad (32)$$

where $(\nabla . \overrightarrow{V^0})_{element}$ is an 8x1 vector which was numerically differentiated.

v. <u>Assembling Element Equations to Obtain Global Equations</u>

The goal was to reach the form:

$$[K]_{system}\{\lambda\} = \{Q\}_{system} \qquad (33)$$

To arrive at this form, a matrix of dimensions n x n for each element was defined where n equals to the total number of nodes in the system. In this matrix, locations corresponding to the nodes of each element were filled appropriately. Then $[K]_{system}$ was obtained by superposition of these element matrices i.e.:

$$[K]_{system} = \sum_{i=1}^{nElements}[K_i] \qquad (34)$$

Similarly, $\{Q\}_{system}$ of dimensions n x 1 was obtained as follows:

$$[Q]_{system} = \sum_{i=1}^{nElements}[Q_i] \qquad (35)$$

vi. <u>Applying Boundary Conditions and Solving</u>

After setting the normal component of the velocity at the no-flow-through boundaries to zero, the system of equations was solved using the iterative Gauss-Seidel method with an over-relaxation factor of 1.8, where iterations would terminate when the maximum relative

percentage error between any two consecutive iterations gets below 2 %. After solving for λ, the adjusted velocities were computed as well as the new divergence. Concerning the optimum alpha ratio that would result in the minimum total residual divergence, following Sherman et al. and Kitada et al. [16, 17], α_1 was set to $\frac{1}{\sqrt{2}}$ and α_3 was increased from 10^{-5} to 10 by factors of 10.

CHAPTER III

RESULTS AND DISCUSSION

In this chapter, statistical results of the WRF-UCM tuning process will be presented and optimum values for the roof albedo, wall albedo, roof thermal conductivity, and AH will be concluded. Additionally, the optimum alpha ratio that resulted in the minimal total residual divergence will be presented.

A. Results of WRF-UCM Calibration

Since the calibration process required performing a lot of simulations, an ID number and a name was given to each simulation. For each of the seasons studied a table containing the ID number for each simulation as well as its name, which briefly describes the parameter changed in that simulation, was constructed (Table 4, 7, 10, and 13).

As can be seen in these tables, the first two simulations didn't include any tuning because the purpose of these simulations was to compare their results with those produced by the tuned UCM. As for the remaining simulations, it is clearly shown that for the roof albedo, increments of 0.01 were used between 0 and 0.1 where the representative value of roofs in Beirut was expected whereas non-uniform increments were used between 0.1 and 0.3. Additionally, similar increments were used for the wall albedo. Moreover, increments of $10 \, W/m^2$ and $0.1 \, W/m.^0K$ were used for AH and the roof thermal conductivity respectively. It is worth noting that the starting value for "kroof" simulations is 0.3 because according to the Thermal Standard for Buildings in Lebanon [31], which was

Simulation	ID	Simulation	ID	Simulation	ID	Simulation	ID
no UCM	1	wallAlbedo_0.04	18	AH_340	35	AH_510	52
UCM default	2	wallAlbedo_0.05	19	AH_350	36	AH_520	53
roofAlbedo_0.01	3	wallAlbedo_0.06	20	AH_360	37	AH_530	54
roofAlbedo_0.02	4	wallAlbedo_0.07	21	AH_370	38	AH_540	55
roofAlbedo_0.03	5	wallAlbedo_0.08	22	AH_380	39	AH_550	56
roofAlbedo_0.04	6	wallAlbedo_0.09	23	AH_390	40	AH_560	57
roofAlbedo_0.05	7	wallAlbedo_0.10	24	AH_400	41	AH_570	58
roofAlbedo_0.06	8	wallAlbedo_0.275	25	AH_410	42	kroof_0.3	59
roofAlbedo_0.07	9	AH_250	26	AH_420	43	kroof_0.4	60
roofAlbedo_0.08	10	AH_260	27	AH_430	44	kroof_0.5	61
roofAlbedo_0.09	11	AH_270	28	AH_440	45	kroof_0.6	62
roofAlbedo_0.1	12	AH_280	29	AH_450	46	kroof_0.7	63
roofAlbedo_0.225	13	AH_290	30	AH_460	47	kroof_0.8	64
roofAlbedo_0.3	14	AH_300	31	AH_470	48	kroof_0.9	65
wallAlbedo_0.01	15	AH_310	32	AH_480	49	kroof_1.0	66
wallAlbedo_0.02	16	AH_320	33	AH_490	50		
wallAlbedo_0.03	17	AH_330	34	AH_500	51		

published in 2010, the maximum allowable roof U-value is $0.71 \, W/m^{2\,0}K$ which corresponds to a maximum thermal conductivity of $0.23 \, W/m^{0}K$; thus, it was a fair assumption that the average thermal conductivity of buildings' roofs in Beirut is above this value given that the majority of buildings in Beirut were built before 2010.

Table 5 which shows statistical results for July simulations indicates that the absolute value of the mean bias, the RMSE, and the NRMSE were higher when no AH was introduced. In addition to that, all temperature simulations during this month showed a cold bias (negative mean bias) indicating that simulated temperatures were generally lower than observed ones. Furthermore, in the simulations in which the roof albedo and the wall albedo were tuned, the higher the tested value was, the higher the RMSE and the absolute value of the mean bias were. Unlike the roof and wall albedos, increasing values of AH resulted in a

Table 5: Statistical parameters for the simulated temperatures during July 2017

	ID	Mean	Std dev	Mean Bias	RMSE	NRMSE	CC
				Temperature			
Average Values for All Stations	1	27.22	1.82	-2.23	2.55	0.094	0.75
	2	27.10	1.68	-2.35	2.64	0.097	0.74
	3	27.36	1.72	-2.09	2.42	0.088	0.74
	4	27.35	1.71	-2.10	2.42	0.088	0.73
	5	27.35	1.71	-2.10	2.42	0.089	0.73
	6	27.34	1.71	-2.11	2.43	0.089	0.73
	7	27.27	1.68	-2.18	2.49	0.091	0.74
	8	27.26	1.68	-2.19	2.49	0.091	0.74
	9	27.24	1.69	-2.21	2.50	0.092	0.74
	10	27.25	1.68	-2.20	2.50	0.092	0.74
	11	27.24	1.68	-2.21	2.51	0.092	0.74
	12	27.23	1.67	-2.22	2.51	0.092	0.74
	13	27.19	1.63	-2.26	2.54	0.093	0.75
	14	27.07	1.52	-2.37	2.62	0.097	0.75
	15	27.36	1.71	-2.09	2.42	0.088	0.73
	16	27.36	1.71	-2.09	2.42	0.088	0.73
	17	27.35	1.72	-2.10	2.42	0.088	0.74
	18	27.35	1.71	-2.10	2.42	0.089	0.73
	19	27.34	1.71	-2.11	2.43	0.089	0.74
	20	27.33	1.72	-2.12	2.44	0.089	0.73
	21	27.33	1.70	-2.12	2.44	0.089	0.73
	22	27.32	1.71	-2.13	2.45	0.090	0.73
	23	27.32	1.70	-2.13	2.45	0.090	0.73
	24	27.31	1.71	-2.14	2.46	0.090	0.73
	25	27.24	1.69	-2.21	2.51	0.092	0.73
	26	27.83	1.77	-1.62	2.05	0.074	0.75
	27	27.84	1.80	-1.61	2.04	0.073	0.75
	28	27.87	1.80	-1.58	2.03	0.073	0.75
	29	27.88	1.80	-1.57	2.02	0.073	0.75
	30	27.91	1.81	-1.54	2.00	0.072	0.75
	31	27.93	1.81	-1.52	1.99	0.071	0.75
	32	27.95	1.82	-1.50	1.97	0.071	0.75
	33	27.96	1.83	-1.48	1.97	0.070	0.75
	34	27.99	1.83	-1.46	1.95	0.070	0.75
	35	28.01	1.84	-1.44	1.94	0.069	0.75
	36	28.03	1.85	-1.42	1.93	0.069	0.75
	37	28.06	1.86	-1.39	1.91	0.068	0.75
	38	28.07	1.86	-1.38	1.90	0.068	0.75
	39	28.09	1.87	-1.36	1.89	0.067	0.76
	40	28.10	1.88	-1.35	1.88	0.067	0.76
	41	28.13	1.88	-1.32	1.87	0.067	0.76
	42	28.14	1.89	-1.31	1.86	0.066	0.76
	43	28.16	1.90	-1.29	1.86	0.066	0.76
	44	28.18	1.90	-1.27	1.85	0.066	0.75
	45	28.19	1.90	-1.26	1.84	0.065	0.75
	46	28.22	1.91	-1.23	1.82	0.065	0.76
	47	28.24	1.92	-1.21	1.82	0.064	0.75
	48	28.25	1.93	-1.20	1.81	0.064	0.76
	49	28.27	1.93	-1.18	1.81	0.064	0.75
	50	28.29	1.94	-1.16	1.80	0.063	0.76
	51	28.31	1.94	-1.14	1.78	0.063	0.76
	52	28.33	1.95	-1.12	1.77	0.063	0.76
	53	28.34	1.96	-1.11	1.77	0.063	0.76
	54	28.36	1.96	-1.09	1.76	0.062	0.76
	55	28.38	1.97	-1.07	1.76	0.062	0.76
	56	28.39	1.98	-1.06	1.75	0.062	0.76
	57	28.41	1.99	-1.04	1.75	0.062	0.76
	58	28.42	1.99	-1.03	1.74	0.061	0.76
	59	28.18	2.02	-1.27	1.90	0.067	0.75
	60	28.19	2.02	-1.26	1.89	0.067	0.75
	61	28.18	2.02	-1.27	1.90	0.068	0.74
	62	28.18	2.02	-1.27	1.91	0.068	0.74
	63	28.20	2.04	-1.25	1.90	0.068	0.74
	64	28.19	2.02	-1.26	1.90	0.068	0.74
	65	28.20	2.03	-1.25	1.91	0.068	0.73
	66	28.21	2.04	-1.24	1.90	0.067	0.74

Table 6: Statistical parameters for the simulated wind speeds during July 2017

	ID	Mean	Std dev	Mean Bias	RMSE	NRMSE	CC
				Wind Speed			
Average Values for All Stations	1	2.55	1.33	1.37	2.05	0.805	0.38
	2	2.58	1.38	1.40	2.08	0.808	0.39
	3	2.47	1.22	1.29	1.94	0.786	0.38
	4	2.45	1.22	1.27	1.93	0.790	0.38
	5	2.45	1.19	1.27	1.92	0.784	0.38
	6	2.43	1.20	1.25	1.92	0.788	0.38
	7	2.36	1.22	1.18	1.87	0.794	0.39
	8	2.37	1.19	1.19	1.87	0.790	0.38
	9	2.37	1.19	1.19	1.88	0.794	0.38
	10	2.37	1.20	1.19	1.88	0.793	0.38
	11	2.34	1.19	1.16	1.86	0.795	0.37
	12	2.33	1.19	1.15	1.85	0.793	0.38
	13	2.28	1.16	1.10	1.81	0.796	0.37
	14	2.21	1.12	1.03	1.77	0.800	0.37
	15	2.46	1.20	1.28	1.93	0.784	0.38
	16	2.45	1.21	1.28	1.92	0.783	0.39
	17	2.46	1.21	1.28	1.94	0.787	0.38
	18	2.45	1.19	1.27	1.92	0.784	0.38
	19	2.45	1.20	1.27	1.92	0.787	0.38
	20	2.46	1.18	1.28	1.92	0.782	0.38
	21	2.44	1.20	1.26	1.92	0.787	0.38
	22	2.41	1.22	1.23	1.90	0.791	0.38
	23	2.41	1.21	1.23	1.91	0.792	0.37
	24	2.41	1.22	1.23	1.92	0.794	0.37
	25	2.35	1.21	1.17	1.87	0.797	0.38
	26	3.29	1.19	2.11	2.52	0.765	0.40
	27	3.31	1.19	2.13	2.53	0.765	0.41
	28	3.33	1.20	2.15	2.55	0.766	0.41
	29	3.35	1.21	2.17	2.57	0.768	0.40
	30	3.36	1.20	2.18	2.58	0.767	0.41
	31	3.38	1.21	2.20	2.60	0.768	0.41
	32	3.40	1.21	2.22	2.61	0.768	0.41
	33	3.42	1.22	2.24	2.63	0.769	0.41
	34	3.44	1.22	2.26	2.65	0.770	0.41
	35	3.46	1.21	2.28	2.67	0.770	0.41
	36	3.49	1.22	2.31	2.69	0.772	0.41
	37	3.50	1.22	2.32	2.70	0.771	0.41
	38	3.52	1.22	2.34	2.72	0.772	0.41
	39	3.54	1.24	2.36	2.74	0.774	0.40
	40	3.56	1.23	2.38	2.75	0.774	0.41
	41	3.58	1.24	2.40	2.77	0.775	0.41
	42	3.58	1.23	2.41	2.78	0.774	0.41
	43	3.62	1.24	2.44	2.80	0.775	0.41
	44	3.63	1.24	2.45	2.82	0.777	0.41
	45	3.64	1.25	2.46	2.83	0.777	0.41
	46	3.65	1.26	2.48	2.85	0.779	0.40
	47	3.67	1.26	2.50	2.87	0.780	0.40
	48	3.69	1.26	2.51	2.88	0.780	0.40
	49	3.71	1.27	2.53	2.90	0.781	0.40
	50	3.73	1.27	2.55	2.91	0.781	0.40
	51	3.74	1.26	2.56	2.92	0.781	0.40
	52	3.76	1.28	2.58	2.94	0.783	0.40
	53	3.77	1.28	2.59	2.95	0.783	0.40
	54	3.79	1.28	2.61	2.97	0.784	0.40
	55	3.81	1.28	2.63	2.98	0.784	0.40
	56	3.83	1.28	2.65	3.01	0.785	0.40
	57	3.84	1.29	2.66	3.02	0.786	0.40
	58	3.86	1.30	2.68	3.04	0.787	0.40
	59	3.31	1.22	2.14	2.56	0.773	0.37
	60	3.31	1.21	2.13	2.55	0.773	0.37
	61	3.31	1.21	2.13	2.55	0.772	0.37
	62	3.31	1.20	2.13	2.55	0.772	0.37
	63	3.32	1.19	2.14	2.55	0.770	0.37
	64	3.30	1.21	2.13	2.55	0.773	0.36
	65	3.31	1.18	2.13	2.55	0.770	0.36
	66	3.32	1.19	2.14	2.55	0.770	0.37

generally decreasing mean bias (in absolute value) and RMSE which attained minimum values of -1.03 ^{0}C and 1.74 ^{0}C at AH equals to 570 W/m^2. As for "kroof" simulations, no significant changes in statistical parameters occurred where the maximum change in the mean bias was 0.03 ^{0}C in absolute value and the RMSE was on average equal to 1.90 ^{0}C. Concerning the wind speed (Table 6), a generally opposite behavior to that of temeprature was observed where the MB and RMSE were higher after introducing AH; however, the NRMSE was generally lower than when no AH was used. In contrary to the temperature, simulated winds showed warm bias (positive mean bias) meaning that they were generally higher than observed wind speeds. Moreover, in the simulations in which AH was calibrated, the change in the root mean square error between the lowest and highest values of AH was 0.52 m/s and that of the mean bias was 0.57 m/s. Another notable observation is that the values of the NRMSE for the first two simulations (noUCM and UCMdefault) were the highest among all other wind speed simulations. In terms of the correlation coefficient, the difference between simulated temeperatures and wind speeds is obvious and as expected due to the randomness and instability of the wind when compared to temeprature which is more stable.

As can be seen in Table 8 and 9, simulated temperatures exhibited a cold bias during most of the simulations indicating that WRF-UCM underestimated temperatures. However, the model started to overestimate simulated temperatures when AH was set to 280 W/m^2 and higher. Additionally, the RMSE showed a general decreasing trend reaching a minimum of 1.22 ^{0}C when AH was set to 160 W/m^2 while slight fluctuations were observed when AH

was increased beyond this value. Unlike the RMSE, the CC showed much less variations where its value ranged between 0.68 and 0.72.

Table 7: Simulations performed during October 2017

Simulation	ID	Simulation	ID
no UCM	1	AH_180	36
UCM default	2	AH_190	37
roofAlbedo_0.01	3	AH_200	38
roofAlbedo_0.02	4	AH_210	39
roofAlbedo_0.03	5	AH_220	40
roofAlbedo_0.04	6	AH_230	41
roofAlbedo_0.05	7	AH_240	42
roofAlbedo_0.06	8	AH_250	43
roofAlbedo_0.07	9	AH_260	44
roofAlbedo_0.08	10	AH_270	45
roofAlbedo_0.09	11	AH_280	46
roofAlbedo_0.1	12	AH_290	47
wallalbedo_0.01	13	AH_300	48
wallalbedo_0.02	14	AH_310	49
wallalbedo_0.03	15	AH_320	50
wallalbedo_0.04	16	AH_330	51
wallalbedo_0.05	17	AH_340	52
wallalbedo_0.06	18	AH_350	53
wallalbedo_0.07	19	AH_360	54
wallalbedo_0.08	20	AH_370	55
wallalbedo_0.09	21	AH_380	56
wallalbedo_0.1	22	AH_390	57
AH_50	23	AH_400	58
AH_60	24	AH_410	59
AH_70	25	AH_420	60
AH_80	26	AH_430	61
AH_90	27	AH_440	62
AH_100	28	kroof_0.3	63
AH_110	29	kroof_0.4	64
AH_120	30	kroof_0.5	65
AH_130	31	kroof_0.6	66
AH_140	32	kroof_0.7	67
AH_150	33	kroof_0.8	68
AH_160	34	kroof_0.9	69
AH_170	35	kroof_1.0	70

Table 8: Statistical parameters for the simulated temperatures during October 2017

Average Values for All Stations

ID	Mean	Std dev	Mean Bias	RMSE	NRMSE	CC
1	23.37	1.40	-0.66	1.39	0.060	0.70
2	23.25	1.40	-0.78	1.45	0.062	0.70
3	23.29	1.36	-0.74	1.39	0.060	0.72
4	23.29	1.35	-0.73	1.39	0.060	0.72
5	23.29	1.36	-0.74	1.39	0.060	0.71
6	23.29	1.35	-0.74	1.39	0.060	0.72
7	23.28	1.35	-0.74	1.40	0.060	0.71
8	23.28	1.35	-0.74	1.39	0.060	0.72
9	23.27	1.36	-0.76	1.40	0.060	0.72
10	23.27	1.35	-0.76	1.41	0.060	0.71
11	23.27	1.35	-0.76	1.41	0.061	0.71
12	23.27	1.35	-0.76	1.41	0.061	0.71
13	23.35	1.34	-0.67	1.35	0.058	0.72
14	23.33	1.34	-0.69	1.37	0.059	0.71
15	23.33	1.34	-0.69	1.37	0.059	0.71
16	23.34	1.34	-0.68	1.35	0.058	0.72
17	23.34	1.35	-0.69	1.36	0.058	0.72
18	23.34	1.33	-0.69	1.36	0.058	0.72
19	23.33	1.34	-0.70	1.36	0.058	0.72
20	23.32	1.35	-0.70	1.37	0.059	0.72
21	23.31	1.35	-0.71	1.38	0.059	0.72
22	23.32	1.34	-0.71	1.37	0.059	0.72
23	23.54	1.31	-0.49	1.28	0.054	0.71
24	23.56	1.31	-0.46	1.27	0.054	0.71
25	23.60	1.31	-0.42	1.26	0.053	0.70
26	23.62	1.31	-0.40	1.26	0.053	0.70
27	23.65	1.31	-0.37	1.25	0.053	0.70
28	23.68	1.31	-0.35	1.25	0.053	0.70
29	23.71	1.30	-0.32	1.24	0.052	0.70
30	23.72	1.31	-0.30	1.24	0.052	0.69
31	23.75	1.30	-0.28	1.24	0.052	0.69
32	23.77	1.30	-0.26	1.24	0.052	0.69
33	23.79	1.30	-0.23	1.23	0.052	0.69
34	23.82	1.30	-0.21	1.22	0.051	0.69
35	23.83	1.31	-0.19	1.23	0.052	0.69
36	23.86	1.31	-0.17	1.24	0.052	0.68
37	23.87	1.30	-0.15	1.23	0.052	0.68
38	23.90	1.31	-0.13	1.23	0.052	0.68
39	23.92	1.31	-0.11	1.23	0.051	0.68
40	23.93	1.31	-0.09	1.23	0.052	0.68
41	23.96	1.31	-0.07	1.23	0.051	0.68
42	23.97	1.31	-0.06	1.23	0.051	0.68
43	23.99	1.31	-0.04	1.24	0.052	0.68
44	24.01	1.32	-0.02	1.23	0.051	0.68
45	24.03	1.32	0.00	1.24	0.051	0.68
46	24.05	1.32	0.02	1.23	0.051	0.68
47	24.06	1.32	0.03	1.23	0.051	0.68
48	24.07	1.32	0.05	1.23	0.051	0.68
49	24.09	1.33	0.07	1.23	0.051	0.68
50	24.11	1.33	0.08	1.24	0.051	0.68
51	24.12	1.33	0.10	1.24	0.051	0.68
52	24.14	1.33	0.11	1.24	0.051	0.68
53	24.15	1.34	0.12	1.25	0.052	0.68
54	24.16	1.34	0.14	1.25	0.052	0.68
55	24.18	1.34	0.15	1.25	0.052	0.68
56	24.19	1.34	0.17	1.26	0.052	0.68
57	24.21	1.35	0.19	1.25	0.052	0.69
58	24.22	1.35	0.19	1.26	0.052	0.68
59	24.24	1.35	0.22	1.26	0.052	0.68
60	24.25	1.36	0.22	1.26	0.052	0.68
61	24.27	1.36	0.24	1.27	0.052	0.68
62	24.28	1.36	0.26	1.26	0.052	0.69
63	24.04	1.32	0.02	1.23	0.051	0.68
64	24.05	1.31	0.03	1.23	0.051	0.68
65	24.04	1.32	0.02	1.23	0.051	0.68
66	24.05	1.31	0.02	1.24	0.051	0.68
67	24.04	1.32	0.02	1.24	0.051	0.68
68	24.05	1.31	0.03	1.24	0.052	0.68
69	24.04	1.32	0.02	1.24	0.052	0.68
70	24.05	1.31	0.03	1.23	0.051	0.68

Table 9: Statistical parameters for the simulated wind speeds during October 2017

Average Values for All Stations

ID	Mean	Std dev	Mean Bias	RMSE	NRMSE	CC
1	3.07	2.05	1.66	2.47	0.803	0.42
2	3.10	2.15	1.69	2.54	0.818	0.41
3	2.71	1.83	1.30	2.08	0.769	0.43
4	2.70	1.84	1.28	2.09	0.775	0.42
5	2.71	1.82	1.30	2.08	0.768	0.43
6	2.72	1.81	1.31	2.08	0.765	0.43
7	2.69	1.82	1.28	2.07	0.769	0.43
8	2.70	1.82	1.29	2.07	0.768	0.43
9	2.67	1.82	1.26	2.06	0.772	0.42
10	2.67	1.82	1.26	2.06	0.770	0.43
11	2.68	1.81	1.27	2.06	0.767	0.43
12	2.69	1.81	1.28	2.06	0.766	0.43
13	2.74	1.84	1.32	2.11	0.771	0.42
14	2.73	1.84	1.32	2.10	0.769	0.43
15	2.72	1.84	1.31	2.10	0.771	0.42
16	2.75	1.83	1.34	2.11	0.768	0.42
17	2.71	1.85	1.30	2.10	0.774	0.42
18	2.73	1.83	1.32	2.10	0.770	0.43
19	2.72	1.83	1.31	2.10	0.773	0.42
20	2.73	1.83	1.32	2.10	0.768	0.43
21	2.74	1.83	1.33	2.10	0.768	0.42
22	2.70	1.84	1.29	2.09	0.773	0.42
23	3.02	1.84	1.61	2.34	0.775	0.38
24	3.08	1.84	1.67	2.38	0.774	0.37
25	3.13	1.85	1.72	2.44	0.778	0.36
26	3.18	1.85	1.77	2.48	0.778	0.36
27	3.24	1.84	1.82	2.51	0.777	0.35
28	3.29	1.86	1.88	2.57	0.782	0.35
29	3.32	1.86	1.91	2.60	0.783	0.35
30	3.36	1.86	1.95	2.63	0.784	0.33
31	3.40	1.87	1.99	2.68	0.787	0.33
32	3.46	1.87	2.05	2.73	0.788	0.31
33	3.49	1.87	2.08	2.76	0.789	0.31
34	3.53	1.88	2.12	2.79	0.789	0.31
35	3.57	1.88	2.16	2.82	0.790	0.31
36	3.61	1.88	2.20	2.86	0.791	0.31
37	3.65	1.88	2.24	2.88	0.790	0.31
38	3.67	1.89	2.26	2.91	0.793	0.30
39	3.71	1.89	2.30	2.94	0.792	0.30
40	3.73	1.90	2.32	2.96	0.794	0.30
41	3.78	1.89	2.37	3.00	0.793	0.31
42	3.81	1.90	2.40	3.03	0.795	0.30
43	3.84	1.89	2.43	3.05	0.793	0.31
44	3.87	1.89	2.46	3.08	0.794	0.30
45	3.90	1.89	2.49	3.10	0.795	0.30
46	3.94	1.90	2.53	3.14	0.797	0.29
47	3.97	1.91	2.55	3.16	0.796	0.30
48	3.98	1.91	2.57	3.17	0.797	0.30
49	3.99	1.93	2.58	3.19	0.801	0.29
50	4.03	1.93	2.62	3.22	0.800	0.30
51	4.07	1.91	2.66	3.25	0.798	0.29
52	4.10	1.92	2.69	3.27	0.799	0.30
53	4.11	1.92	2.70	3.29	0.800	0.29
54	4.15	1.90	2.74	3.31	0.797	0.30
55	4.18	1.91	2.77	3.34	0.798	0.30
56	4.19	1.90	2.78	3.34	0.796	0.31
57	4.22	1.91	2.81	3.37	0.798	0.30
58	4.23	1.92	2.82	3.38	0.799	0.30
59	4.27	1.90	2.86	3.41	0.798	0.30
60	4.29	1.91	2.88	3.43	0.799	0.30
61	4.31	1.92	2.89	3.45	0.801	0.30
62	4.33	1.91	2.92	3.47	0.800	0.30
63	3.93	1.92	2.52	3.14	0.798	0.30
64	3.95	1.89	2.53	3.13	0.794	0.30
65	3.92	1.92	2.50	3.13	0.798	0.29
66	3.93	1.91	2.51	3.13	0.797	0.30
67	3.94	1.91	2.53	3.14	0.797	0.29
68	3.94	1.90	2.53	3.13	0.795	0.30
69	3.94	1.89	2.52	3.13	0.795	0.30
70	3.93	1.90	2.52	3.13	0.795	0.30

In contrary to the temperature, statistical parameters for the wind speed showed an opposite trend where a warm bias (positive mean bias) with a generally increasing trend was observed for all simulations. Similar to the mean bias, the RMSE increased almost monotonically, especially when AH was increased, reaching a maximum of 3.47 m/s while it remained almost constant when variations in the roof thermal conductivity were introduced. Furthermore, the CC fluctuated between 0.29 and 0.43.

Table 10: Simulations performed during January 2017

Simulation	ID	Simulation	ID	Simulation	ID
no UCM	1	AH_280	26	AH_530	51
UCM default	2	AH_290	27	AH_540	52
AH_50	3	AH_300	28	AH_550	53
AH_60	4	AH_310	29	AH_560	54
AH_70	5	AH_320	30	AH_570	55
AH_80	6	AH_330	31	AH_580	56
AH_90	7	AH_340	32	AH_590	57
AH_100	8	AH_350	33	AH_600	58
AH_110	9	AH_360	34	AH_610	59
AH_120	10	AH_370	35	AH_620	60
AH_130	11	AH_380	36	AH_630	61
AH_140	12	AH_390	37	AH_640	62
AH_150	13	AH_400	38	AH_650	63
AH_160	14	AH_410	39	AH_660	64
AH_170	15	AH_420	40	AH_670	65
AH_180	16	AH_430	41	AH_680	66
AH_190	17	AH_440	42	AH_690	67
AH_200	18	AH_450	43	AH_700	68
AH_210	19	AH_460	44	AH_710	69
AH_220	20	AH_470	45	AH_720	70
AH_230	21	AH_480	46		
AH_240	22	AH_490	47		
AH_250	23	AH_500	48		
AH_260	24	AH_510	49		
AH_270	25	AH_520	50		

Table 11: Statistical parameters for the simulated temperatures during January 2017

	ID	Mean	Std dev	Mean Bias	RMSE	NRMSE	CC		ID	Mean	Std dev	Mean Bias	RMSE	NRMSE	CC
Average Values for All Stations	1	13.77	2.77	-1.16	2.16	0.157	0.79	Average Values for All Stations	36	14.60	2.81	-0.34	2.01	0.137	0.76
	2	13.67	2.77	-1.26	2.15	0.157	0.81		37	14.59	2.86	-0.35	2.03	0.139	0.76
	3	13.87	2.76	-1.07	2.12	0.153	0.79		38	14.62	2.83	-0.32	2.01	0.137	0.76
	4	13.92	2.76	-1.01	2.08	0.149	0.79		39	14.64	2.84	-0.30	2.01	0.137	0.76
	5	13.95	2.76	-0.99	2.10	0.150	0.78		40	14.65	2.83	-0.28	2.02	0.138	0.75
	6	13.97	2.78	-0.96	2.09	0.150	0.78		41	14.66	2.85	-0.27	2.01	0.137	0.76
	7	14.01	2.77	-0.93	2.09	0.149	0.78		42	14.66	2.87	-0.27	2.02	0.138	0.76
	8	14.05	2.76	-0.88	2.05	0.146	0.78		43	14.69	2.84	-0.25	2.01	0.137	0.76
	9	14.07	2.77	-0.87	2.06	0.147	0.78		44	14.72	2.83	-0.22	2.00	0.136	0.76
	10	14.09	2.79	-0.85	2.07	0.147	0.78		45	14.70	2.89	-0.24	2.03	0.138	0.75
	11	14.12	2.79	-0.82	2.07	0.146	0.78		46	14.71	2.88	-0.23	2.03	0.138	0.75
	12	14.13	2.80	-0.80	2.07	0.146	0.77		47	14.74	2.88	-0.20	2.01	0.136	0.76
	13	14.18	2.78	-0.76	2.03	0.143	0.78		48	14.75	2.87	-0.18	2.00	0.136	0.76
	14	14.18	2.78	-0.75	2.04	0.144	0.77		49	14.76	2.87	-0.17	2.00	0.136	0.76
	15	14.19	2.81	-0.74	2.06	0.145	0.77		50	14.77	2.88	-0.17	2.02	0.137	0.75
	16	14.21	2.81	-0.72	2.06	0.145	0.77		51	14.79	2.88	-0.14	2.03	0.138	0.75
	17	14.25	2.81	-0.69	2.04	0.143	0.77		52	14.81	2.89	-0.13	2.03	0.137	0.75
	18	14.26	2.81	-0.67	2.05	0.144	0.77		53	14.82	2.89	-0.12	2.03	0.137	0.75
	19	14.28	2.81	-0.65	2.05	0.143	0.77		54	14.82	2.89	-0.11	2.03	0.137	0.75
	20	14.32	2.79	-0.61	2.02	0.141	0.77		55	14.85	2.88	-0.08	2.03	0.137	0.75
	21	14.32	2.84	-0.61	2.04	0.143	0.77		56	14.88	2.86	-0.05	2.00	0.135	0.76
	22	14.32	2.83	-0.61	2.06	0.143	0.76		57	14.87	2.89	-0.07	2.03	0.137	0.75
	23	14.36	2.81	-0.58	2.03	0.141	0.76		58	14.88	2.89	-0.06	2.03	0.137	0.75
	24	14.39	2.81	-0.55	2.02	0.141	0.76		59	14.91	2.87	-0.02	2.00	0.134	0.76
	25	14.41	2.82	-0.53	2.03	0.141	0.76		60	14.90	2.90	-0.04	2.04	0.137	0.75
	26	14.42	2.82	-0.51	2.03	0.140	0.76		61	14.93	2.88	0.00	2.03	0.136	0.75
	27	14.44	2.83	-0.50	2.03	0.141	0.76		62	14.94	2.90	0.00	2.03	0.136	0.75
	28	14.47	2.80	-0.47	2.02	0.139	0.76		63	14.94	2.92	0.00	2.04	0.137	0.75
	29	14.47	2.81	-0.46	2.01	0.139	0.76		64	14.96	2.92	0.03	2.04	0.137	0.75
	30	14.47	2.86	-0.46	2.06	0.142	0.75		65	14.96	2.93	0.02	2.06	0.138	0.75
	31	14.52	2.82	-0.42	2.00	0.138	0.76		66	14.98	2.93	0.04	2.05	0.137	0.75
	32	14.53	2.81	-0.40	2.01	0.138	0.76		67	14.98	2.93	0.04	2.05	0.137	0.75
	33	14.55	2.82	-0.38	2.00	0.138	0.76		68	14.99	2.93	0.06	2.06	0.138	0.75
	34	14.52	2.84	-0.41	2.05	0.141	0.75		69	15.01	2.93	0.08	2.05	0.136	0.75
	35	14.57	2.85	-0.37	2.01	0.138	0.76		70	15.00	2.95	0.06	2.08	0.139	0.75

Table 12: Statistical parameters for the simulated wind speeds during January 2017

	ID	Mean	Std dev	Mean Bias	RMSE	NRMSE	CC		ID	Mean	Std dev	Mean Bias	RMSE	NRMSE	CC
Average Values for All Stations	1	4.39	3.17	2.45	3.54	0.807	0.52	Average Values for All Stations	36	5.22	2.89	3.28	4.14	0.792	0.44
	2	4.59	3.36	2.64	3.74	0.816	0.52		37	5.27	2.90	3.33	4.19	0.794	0.45
	3	4.09	2.94	2.15	3.23	0.790	0.50		38	5.27	2.87	3.33	4.18	0.793	0.43
	4	4.17	2.94	2.23	3.28	0.788	0.49		39	5.27	2.92	3.33	4.19	0.794	0.45
	5	4.18	2.86	2.24	3.26	0.780	0.49		40	5.29	2.87	3.35	4.19	0.792	0.44
	6	4.21	2.92	2.27	3.30	0.783	0.50		41	5.31	2.87	3.37	4.24	0.798	0.42
	7	4.24	2.89	2.30	3.32	0.784	0.48		42	5.38	2.94	3.44	4.31	0.801	0.44
	8	4.31	2.98	2.37	3.42	0.793	0.49		43	5.31	2.88	3.37	4.23	0.798	0.42
	9	4.35	2.92	2.41	3.44	0.790	0.48		44	5.44	2.87	3.50	4.33	0.796	0.43
	10	4.40	2.94	2.46	3.50	0.795	0.47		45	5.43	2.91	3.49	4.33	0.798	0.44
	11	4.44	2.90	2.50	3.49	0.786	0.48		46	5.40	2.91	3.46	4.32	0.800	0.43
	12	4.53	2.97	2.59	3.59	0.793	0.49		47	5.46	2.89	3.52	4.37	0.799	0.42
	13	4.53	2.92	2.59	3.60	0.794	0.45		48	5.47	2.88	3.53	4.35	0.795	0.43
	14	4.51	2.90	2.56	3.56	0.790	0.46		49	5.48	2.90	3.54	4.39	0.800	0.43
	15	4.60	2.95	2.66	3.66	0.796	0.46		50	5.54	2.90	3.60	4.45	0.803	0.42
	16	4.70	2.93	2.75	3.72	0.792	0.46		51	5.51	2.85	3.57	4.39	0.796	0.42
	17	4.70	2.98	2.76	3.73	0.794	0.48		52	5.58	2.88	3.64	4.46	0.799	0.42
	18	4.71	2.92	2.77	3.72	0.790	0.46		53	5.60	2.84	3.65	4.45	0.795	0.43
	19	4.73	2.90	2.79	3.75	0.793	0.45		54	5.58	2.89	3.64	4.48	0.803	0.41
	20	4.77	2.94	2.83	3.77	0.790	0.47		55	5.63	2.89	3.68	4.50	0.801	0.42
	21	4.84	2.92	2.90	3.80	0.785	0.47		56	5.65	2.86	3.71	4.52	0.800	0.41
	22	4.79	2.90	2.85	3.78	0.788	0.46		57	5.68	2.84	3.73	4.52	0.797	0.42
	23	4.86	2.97	2.92	3.86	0.795	0.46		58	5.65	2.83	3.71	4.52	0.799	0.41
	24	4.91	2.90	2.96	3.87	0.788	0.47		59	5.73	2.84	3.79	4.58	0.800	0.41
	25	4.91	2.93	2.97	3.90	0.794	0.46		60	5.71	2.85	3.76	4.55	0.798	0.42
	26	4.93	2.90	2.99	3.90	0.790	0.45		61	5.72	2.86	3.78	4.57	0.798	0.42
	27	5.01	2.94	3.07	3.99	0.797	0.44		62	5.72	2.87	3.78	4.56	0.798	0.43
	28	4.99	2.92	3.05	3.98	0.797	0.43		63	5.70	2.86	3.76	4.55	0.798	0.42
	29	5.03	2.93	3.09	3.99	0.794	0.45		64	5.73	2.84	3.79	4.57	0.798	0.42
	30	5.08	2.93	3.14	4.05	0.796	0.45		65	5.76	2.86	3.82	4.62	0.801	0.42
	31	5.08	2.88	3.14	4.01	0.790	0.44		66	5.80	2.88	3.86	4.63	0.799	0.43
	32	5.11	2.96	3.17	4.10	0.802	0.43		67	5.80	2.85	3.86	4.62	0.797	0.43
	33	5.20	2.98	3.26	4.18	0.804	0.44		68	5.83	2.89	3.88	4.68	0.804	0.42
	34	5.11	2.90	3.17	4.07	0.797	0.43		69	5.80	2.86	3.86	4.63	0.798	0.42
	35	5.22	2.94	3.28	4.17	0.798	0.45		70	5.82	2.89	3.87	4.66	0.801	0.43

During January, Table 11 clearly shows a generally decreasing pattern (in absolute value) in the mean bias during most of the simulations. Unlike the mean bias, the RMSE values exhibited frequent increase and decrease attaining a minimum of 2.00 ^{0}C for multiple values of AH and a maximum of 2.16 ^{0}C when UCM was not coupled with WRF. In addition, it is noteworthy that the RMSE values during January were higher than those obtained during October and July. In terms of correlation, the CC varied between 0.75 and 0.81. As for wind speed (Table 12), both the mean bias and the RMSE increased almost monotonically with increasing values of AH reaching their peaks of 3.88 ^{0}C and 4.68 ^{0}C respetively at AH equals to 700 W/m^2.

Table 13: Simulations performed during April 2017

Simulation	ID	Simulation	ID
no UCM	1	AH_170	19
UCM default	2	AH_180	20
AH_10	3	AH_190	21
AH_20	4	AH_200	22
AH_30	5	AH_210	23
AH_40	6	AH_220	24
AH_50	7	AH_230	25
AH_60	8	AH_240	26
AH_70	9	AH_250	27
AH_80	10	AH_260	28
AH_90	11	AH_270	29
AH_100	12	AH_280	30
AH_110	13	AH_290	31
AH_120	14	AH_300	32
AH_130	15	AH_310	33
AH_140	16	AH_320	34
AH_150	17	AH_330	35
AH_160	18	AH_340	36

Table 14: Statistical parameters for the simulated temperatures during April 2017

	Temperature								Temperature					
ID	Mean	Std dev	Mean Bias	RMSE	NRMSE	CC		ID	Mean	Std dev	Mean Bias	RMSE	NRMSE	CC
1	20.59	4.27	-1.14	2.16	0.105	0.91		19	21.10	4.40	-0.63	1.98	0.094	0.90
2	20.58	4.24	-1.15	2.18	0.106	0.90		20	21.12	4.41	-0.61	1.99	0.094	0.90
3	20.66	4.24	-1.06	2.12	0.102	0.90		21	21.14	4.42	-0.58	1.99	0.094	0.90
4	20.69	4.24	-1.03	2.09	0.101	0.91		22	21.17	4.43	-0.56	1.99	0.094	0.90
5	20.72	4.25	-1.00	2.08	0.100	0.91		23	21.19	4.44	-0.53	1.98	0.094	0.90
6	20.75	4.25	-0.97	2.07	0.100	0.91		24	21.22	4.46	-0.51	1.99	0.094	0.90
7	20.78	4.26	-0.95	2.06	0.099	0.91		25	21.24	4.46	-0.49	1.99	0.094	0.90
8	20.81	4.27	-0.92	2.05	0.098	0.91		26	21.26	4.47	-0.47	1.99	0.093	0.90
9	20.83	4.28	-0.89	2.04	0.098	0.91		27	21.28	4.48	-0.44	1.99	0.093	0.90
10	20.86	4.29	-0.87	2.03	0.097	0.91		28	21.30	4.49	-0.42	1.99	0.093	0.90
11	20.89	4.30	-0.84	2.02	0.097	0.91		29	21.32	4.50	-0.40	1.99	0.093	0.90
12	20.91	4.31	-0.81	2.01	0.096	0.91		30	21.35	4.51	-0.38	1.99	0.093	0.90
13	20.94	4.32	-0.78	2.00	0.096	0.91		31	21.37	4.52	-0.36	1.99	0.093	0.90
14	20.97	4.34	-0.76	2.00	0.095	0.91		32	21.39	4.53	-0.33	1.99	0.093	0.90
15	20.99	4.35	-0.73	2.00	0.095	0.90		33	21.41	4.54	-0.32	2.00	0.093	0.90
16	21.02	4.36	-0.71	1.99	0.095	0.90		34	21.43	4.55	-0.30	2.00	0.093	0.90
17	21.04	4.38	-0.68	1.99	0.095	0.90		35	21.45	4.56	-0.28	2.00	0.093	0.90
18	21.07	4.39	-0.65	1.99	0.094	0.90		36	21.47	4.56	-0.26	2.00	0.093	0.90

Table 15: Statistical parameters for the simulated wind speeds during April 2017

	Wind Speed								Wind Speed					
ID	Mean	Std dev	Mean Bias	RMSE	NRMSE	CC		ID	Mean	Std dev	Mean Bias	RMSE	NRMSE	CC
1	3.91	1.75	2.28	3.07	0.786	0.26		19	4.08	1.57	2.45	3.14	0.771	0.23
2	4.26	1.87	2.63	3.41	0.801	0.22		20	4.10	1.57	2.47	3.16	0.771	0.23
3	3.65	1.60	2.02	2.83	0.774	0.24		21	4.13	1.56	2.50	3.18	0.771	0.23
4	3.68	1.60	2.05	2.85	0.774	0.24		22	4.14	1.55	2.51	3.19	0.771	0.22
5	3.72	1.60	2.08	2.87	0.773	0.24		23	4.17	1.56	2.54	3.21	0.770	0.22
6	3.75	1.59	2.12	2.90	0.772	0.24		24	4.18	1.56	2.55	3.23	0.771	0.22
7	3.78	1.59	2.15	2.92	0.773	0.23		25	4.21	1.55	2.57	3.24	0.771	0.22
8	3.80	1.58	2.17	2.94	0.772	0.24		26	4.22	1.55	2.59	3.26	0.771	0.22
9	3.83	1.58	2.20	2.96	0.773	0.23		27	4.25	1.56	2.62	3.28	0.771	0.22
10	3.86	1.58	2.22	2.98	0.772	0.23		28	4.27	1.56	2.64	3.29	0.771	0.23
11	3.87	1.58	2.24	2.99	0.772	0.23		29	4.29	1.55	2.66	3.30	0.770	0.23
12	3.90	1.58	2.27	3.01	0.772	0.23		30	4.30	1.55	2.67	3.32	0.771	0.23
13	3.93	1.57	2.30	3.03	0.772	0.23		31	4.31	1.56	2.68	3.33	0.772	0.23
14	3.95	1.57	2.32	3.05	0.772	0.23		32	4.34	1.55	2.70	3.34	0.771	0.23
15	3.98	1.57	2.35	3.07	0.772	0.22		33	4.36	1.56	2.73	3.36	0.771	0.23
16	4.00	1.56	2.37	3.09	0.771	0.23		34	4.38	1.55	2.75	3.38	0.771	0.23
17	4.03	1.58	2.40	3.11	0.772	0.23		35	4.40	1.55	2.76	3.39	0.771	0.23
18	4.05	1.57	2.42	3.12	0.772	0.23		36	4.42	1.55	2.79	3.41	0.771	0.23

Simulated temperatures during April (Table 14) revealed a cold bias throughtout all

simulations with a decreasing absolute value of the mean bias reaching a value as low as

- 0.26 ^{0}C. On the other hand, the RMSE decreased from a maximum value of 2.18 ^{0}C reaching a minimum of 1.98 ^{0}C after which a slight increase to a value of 2.00 ^{0}C occurred. Concerning the wind speed, table (Table 15) clearly shows that as the value of AH increased, both the mean bias and the RMSE increased steadily reaching a maximum of 2.79 m/s and 3.41 m/s respectively while the CC remained approximately constant.

In general, during the whole study period, simulated temperatures when no UCM was used and when UCM was used with default parameters (where AH is zero) resulted in higher mean bias (in absolute value) and RMSE values than when AH was included. Besides that, it was noted that the mean bias and RMSE corresponding to simulated wind speeds when UCM with default parameters was used were higher than those corresponding to simulations with no UCM. Furthermore, it can be observed from the tables above that the CC corresponding to the simulated air temperature was higher than that corresponding to the simulated wind speed which is expected given that temperature is more stable than wind speed.

As mentioned in the previous chapter, for each simulation, the NRMSE for both the temperature and wind speed were averaged using the CC's as weights to be able to determine optimum parameters. Therefore, the averaging process resulted in Table 16 where horizontal lines within each table separate simulations with different tuned parameters.

As Table 16 (a) and (b) show, the weighted average NRMSE, hereafter referred to as WA-NRMSE, attained a minimum of 0.3254 and 0.3242 during the months of July and October respectively when the roof albedo was tuned indicating that the roof albedo of 0.03 was the optimum value. The same tables reveal as well that the optimum values of the wall albedo were 0.06 during July and 0.04 during October which correspond to minimum WA-

NRMSE values of 0.3247 and 0.3202 respectively resulting in an average value of 0.05 for the wall albedo.

Concerning the roof thermal conductivity, the optimum value during July was 0.4 $W/m.^0 K$ and that during October was 0.5 $W/m.^0 K$ which correspond to minimum WA-NRMSE values of 0.2992 and 0.2767 respectively and an average value of 0.45 $W/m.^0 K$.

Regarding the anthropogenic heat, the minimum WA-NRMSE during July was 0.3092 which corresponds to AH value of 510 W/m^2. During October, results showed that the optimum AH value was 280 W/m^2 with a minimum WA-NRMSE of 0.2743. As for the remaining months of January and April, optimum AH values were 610 W/m^2 and 210 W/m^2 respectively based on a minimum WA-NRMSE of 0.3676 and 0.2284 during the same respective months. As can be noticed, the highest AH value was in January and the lowest was in April which was expected because in January i.e. the winter season, domestic hot water and heating demands are usually high while in April i.e. the spring season which is characterized by moderate temperatures, almost no heating/cooling is required and dometic hot water demands are usually very low compared to the other months considered in the study. Table 17 below summarizes the optimum values obtained.

Table 16: Weighted mean of the NRMSE for the months of (a) July, (b) October, (c) January, and (d) April

(a)

ID	Weighted Mean NRMSE
1	0.3331
2	0.3415
3	0.3267
4	0.3267
5	0.3254
6	0.3266
7	0.3318
8	0.3288
9	0.3279
10	0.3288
11	0.3276
12	0.3287
13	0.3260
14	0.3275
15	0.3258
16	0.3294
17	0.3274
18	0.3254
19	0.3266
20	0.3247
21	0.3267
22	0.3307
23	0.3277
24	0.3286
25	0.3320
26	0.3149
27	0.3170
28	0.3163
29	0.3161
30	0.3166
31	0.3172
32	0.3167
33	0.3166
34	0.3157
35	0.3152
36	0.3149
37	0.3149
38	0.3154
39	0.3128
40	0.3141
41	0.3135
42	0.3154
43	0.3141
44	0.3147
45	0.3151
46	0.3123
47	0.3135
48	0.3132
49	0.3135
50	0.3136
51	0.3102
52	0.3092
53	0.3114
54	0.3109
55	0.3111
56	0.3102
57	0.3099
58	0.3103
59	0.3014
60	0.2992
61	0.3024
62	0.3011
63	0.3019
64	0.3000
65	0.3008
66	0.3006

(b)

ID	Weighted Mean NRMSE
1	0.3376
2	0.3435
3	0.3260
4	0.3256
5	0.3242
6	0.3246
7	0.3261
8	0.3260
9	0.3251
10	0.3291
11	0.3259
12	0.3276
13	0.3217
14	0.3255
15	0.3224
16	0.3202
17	0.3239
18	0.3237
19	0.3210
20	0.3242
21	0.3219
22	0.3241
23	0.3038
24	0.3020
25	0.3004
26	0.2990
27	0.2955
28	0.2965
29	0.2952
30	0.2906
31	0.2878
32	0.2826
33	0.2811
34	0.2821
35	0.2832
36	0.2836
37	0.2810
38	0.2794
39	0.2792
40	0.2805
41	0.2806
42	0.2791
43	0.2819
44	0.2792
45	0.2776
46	0.2743
47	0.2795
48	0.2777
49	0.2768
50	0.2794
51	0.2770
52	0.2788
53	0.2774
54	0.2797
55	0.2814
56	0.2855
57	0.2799
58	0.2817
59	0.2817
60	0.2819
61	0.2799
62	0.2792
63	0.2771
64	0.2800
65	0.2767
66	0.2785
67	0.2772
68	0.2794
69	0.2781
70	0.2786

(c)

ID	Weighted Mean NRMSE
1	0.4139
2	0.4147
3	0.3990
4	0.3944
5	0.3928
6	0.3951
7	0.3902
8	0.3932
9	0.3911
10	0.3900
11	0.3923
12	0.3957
13	0.3824
14	0.3837
15	0.3897
16	0.3884
17	0.3934
18	0.3869
19	0.3824
20	0.3869
21	0.3874
22	0.3853
23	0.3878
24	0.3858
25	0.3850
26	0.3827
27	0.3827
28	0.3785
29	0.3820
30	0.3862
31	0.3769
32	0.3790
33	0.3811
34	0.3795
35	0.3827
36	0.3794
37	0.3835
38	0.3756
39	0.3815
40	0.3779
41	0.3715
42	0.3800
43	0.3741
44	0.3756
45	0.3812
46	0.3792
47	0.3744
48	0.3757
49	0.3748
50	0.3749
51	0.3749
52	0.3728
53	0.3749
54	0.3726
55	0.3749
56	0.3697
57	0.3739
58	0.3695
59	0.3676
60	0.3742
61	0.3723
62	0.3763
63	0.3739
64	0.3727
65	0.3746
66	0.3781
67	0.3781
68	0.3759
69	0.3749
70	0.3793

(d)

ID	Weighted Mean NRMSE
1	0.2550
2	0.2438
3	0.2446
4	0.2419
5	0.2413
6	0.2401
7	0.2375
8	0.2375
9	0.2331
10	0.2341
11	0.2330
12	0.2325
13	0.2309
14	0.2299
15	0.2287
16	0.2298
17	0.2298
18	0.2296
19	0.2292
20	0.2292
21	0.2295
22	0.2288
23	0.2284
24	0.2288
25	0.2287
26	0.2286
27	0.2286
28	0.2296
29	0.2316
30	0.2300
31	0.2297
32	0.2310
33	0.2331
34	0.2316
35	0.2310
36	0.2317

Table 17: Optimum parameters obtained from the tuning process

Parameter	July	October	January	April	Average
roof albedo	0.03	0.03	-	-	0.03
wall albedo	0.06	0.04	-	-	0.05
roof thermal conductivity	0.4	0.5	-	-	0.45
AH	510	280	610	210	402.5

To examine the difference between the simulations in which no UCM was used (noUCM), the ones where UCM was used with its default parameters (UCMdefault), and the ones in which optimized parameters were used (UCMOptimized), average simulated temperatures at all stations and during all studied periods were plotted against observed temperatures (Obs) that were averaged over all stations as can be seen in Figure 7 (a - d).

(a)
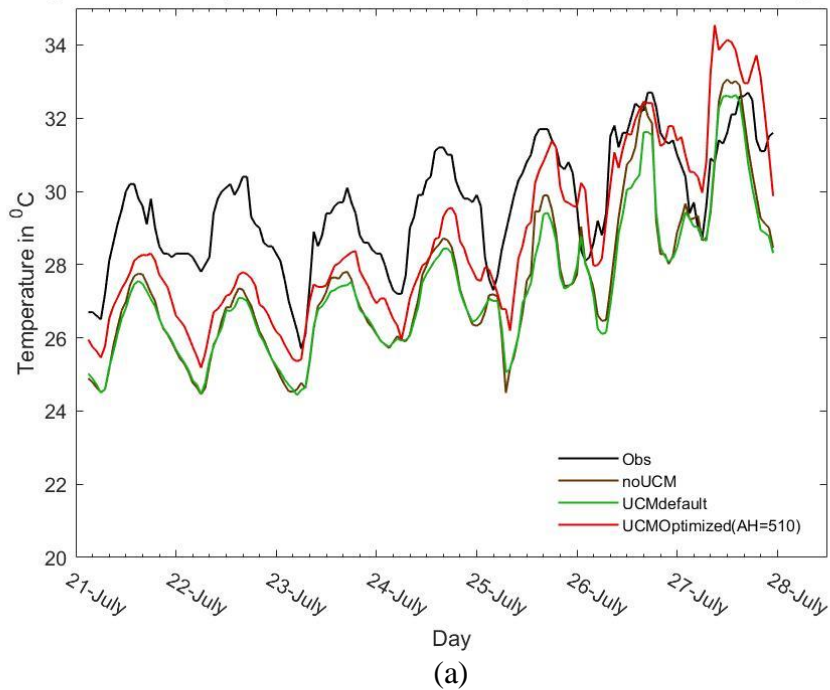
Average Simulated Temperature Versus Observed Temperature at All Stations During October 2017

(b)

Average Simulated Temperature Versus Observed Temperature at All Stations During January 2017

(c)

46

Average Simulated Temperature Versus Observed Temperature at All Stations During April 2017

(d)
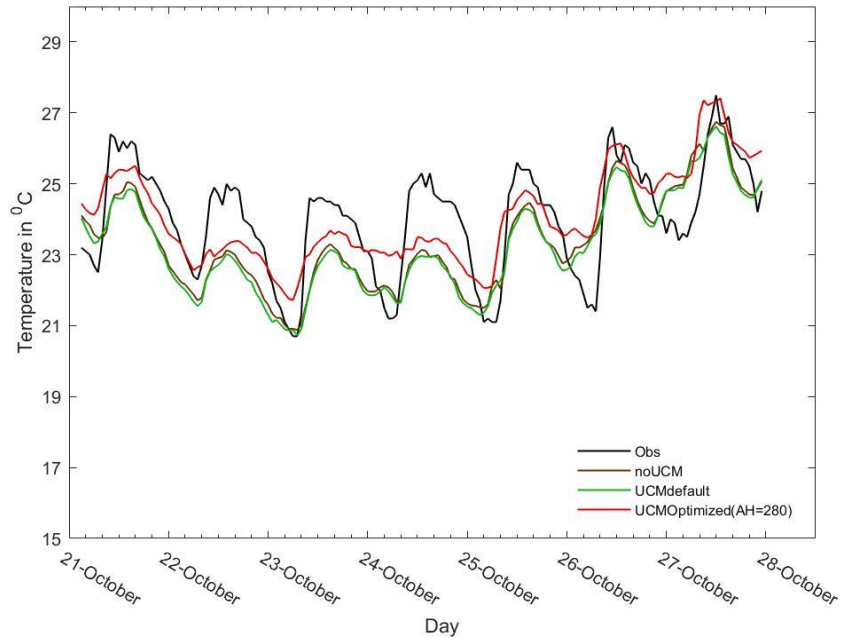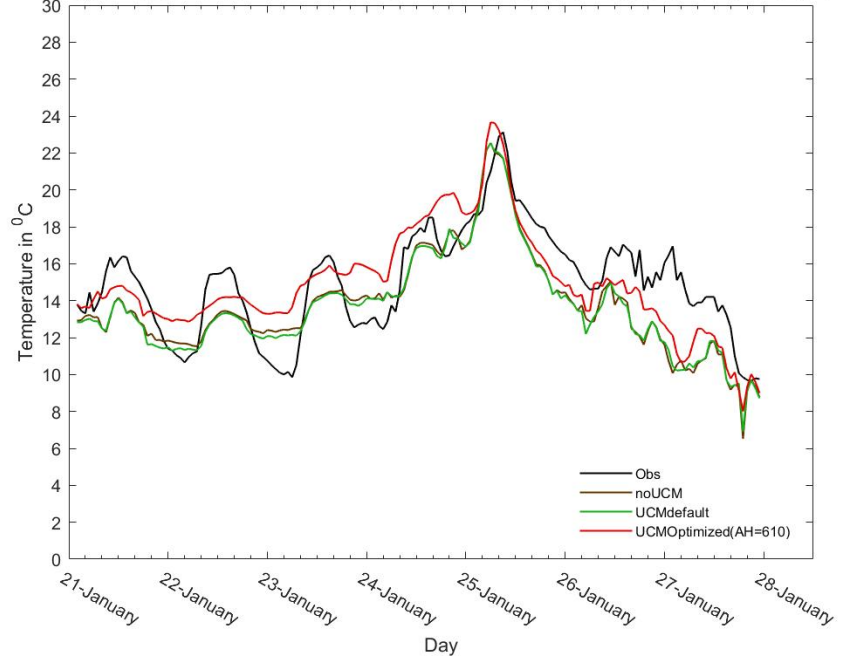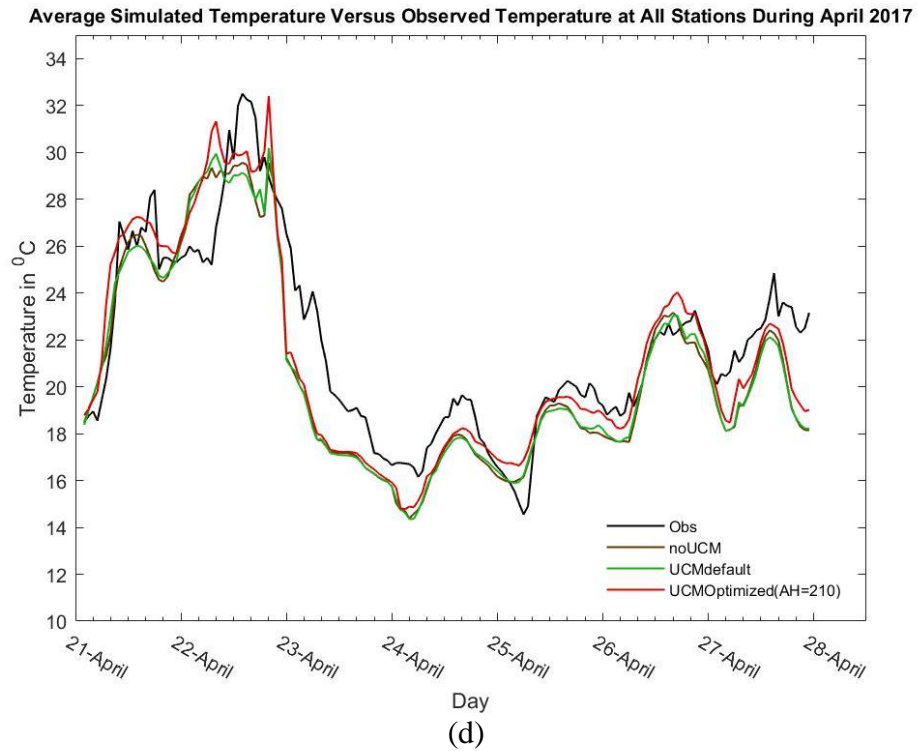
Figure 7: Comparison between average observed temperature and average simulated temperature with different permutations of UCM during (a) July (b) October (c) January and (d) April in the year 2017

As can be clearly noticed in the figures above, all simulations produced a temperature profile that generally resembles that produced by observations especially during the morning of January 25th in which a temperature peak was observed and during April 23rd in which a noticeable temperature drop occurred. In addition, it is vivid that UCMOptimized produced a temperature profile that is generally higher than that produced by noUCM and UCMdefault simulations with the difference being generally higher during all months except in April where the different simulations produced very similar values particularly during the period from April 22nd evening till April 24th noon. Furthermore, the graph of October shows

47

that in general, UCMOptimized was able to capture the average observed temperatures during most of the days that were studied.

To examine the differences between the different UCM permutations in more details, Table 18 which contains the Average, Mean Bias, RMSE, and CC was constructed. Results showed that except for the UCMOptimized simulation during October, a cold bias was observed for all other simulations with a minimum of 0.02 ^{0}C and a maximum of 2.28 ^{0}C in absolute value. Furthermore, results confirm again the observations made earlier that results obtained from the UCMdefault simulations are the least accurate since the absolute value of the mean bias and the RMSE were the highest during the four months compared to noUCM and UCMOptimized simulations. Additionally, it can be noticed that UCMOptimized simulation during October produced temperatures with highest accuracy when compared to observations where the Mean bias, RMSE, and NRMSE values were 0.02 ^{0}C, 1.07 ^{0}C, and 0.04 respectively. Also, comparing UCMOptimized simulations for all months shows that the one performed during Januray produced the highest NRMSE (0.13) which is attributed to the fact that wind speeds during this month are the highest when compared to those during the other three months. A closer look at the differences in the average error (mean bias) between the three UCM permutations shows that the highest differences occurred in July and January where UCMOptimized resulted in an improved simulated temepratures by 1.19 ^{0}C and 1.34 ^{0}C during July and by 1.14 ^{0}C and 1.24 ^{0}C during January when compared to noUCM and UCMdefault simulations respectively. A common notable parameter for all simulations during all months is the correlation coefficient which was relatively high during all months reaching a value as high as 0.91 during April.

Table 18: Statistical parameters for the average temperatures during July, October, January and April in the year 2017

		Average	Mean Bias	RMSE	NRMSE	CC
July	Obs	29.63				
	noUCM	27.50	-2.13	2.43	0.09	0.83
	UCMdefault	27.35	-2.28	2.53	0.09	0.82
	UCMOptimized(AH=510)	28.69	-0.94	1.63	0.06	0.83
October	Obs	24.03				
	noUCM	23.37	-0.66	1.25	0.05	0.74
	UCMdefault	23.25	-0.78	1.31	0.06	0.74
	UCMOptimized(AH=280)	24.05	0.02	1.07	0.04	0.73
January	Obs	14.93				
	noUCM	13.77	-1.16	2.11	0.15	0.80
	UCMdefault	13.67	-1.26	2.10	0.15	0.82
	UCMOptimized(AH=610)	14.91	-0.02	1.93	0.13	0.77
April	Obs	21.73				
	noUCM	20.59	-1.14	2.06	0.10	0.91
	UCMdefault	20.58	-1.15	2.09	0.10	0.91
	UCMOptimized(AH=210)	21.19	-0.53	1.90	0.09	0.91

To further study the difference between simulations in which no UCM was used and those in which UCM was used with optimized parameters during different times of the day, simulated temperatures at 8:00 a.m., 12:00 p.m., and 8:00 p.m. were averaged over all 7 days during each of the 4 months studied and heat maps in Figure 8, 9, 10, and 11were produced where the first column represents noUCM temperature contours, the second column represents contours produced by UCMOptimized and third column represents the difference between UCMOptimized and noUCM temperature values (UCMOptimized minus noUCM).

As can be seen in the figures, a significant difference in temperature between noUCM and UCMOptimized simulations exists at 8:00 a.m. and 8:00 p.m. for all simulated months while there is no noticeable change at noon indicating that both simulations produce comparable results at this time. In addition, it is clearly shown that the fine – tuned UCM with optimum parameters is capable of producing the urban heat island effect during early

morning and evening unlike the case when UCM is not coupled with WRF. In fact, the high temperature contours produced by UCMOptimized at 8:00 a.m. and 8:00 p.m. during the simulated months are located over *Dawra*, a highly dense urban area in Beirut. During the morning of July, an average temperature difference of about 1 ^{0}C was observed while approximately an average difference of 1.2 ^{0}C was observed in the evening. As for October, average temperature differences between both simulations were approximately 2.1 ^{0}C and 1.1 ^{0}C at 8:00 a.m. and 8:00 p.m. respectively. Similarly, the morning difference was higher in January where it reached an average value of about 2.7 ^{0}C while that during the evening was higher than that in October by about 0.6 ^{0}C. Additionally, in April, the average evening difference was higher than that during early morning where it reached an average of about 0.5 ^{0}C during early morning and 1.2 ^{0}C during the evening. Moreover, a distinguishing observation in July and April is that at noon, noUCM produced higher values than UCMOptimized resulting in negative temeprature differences over Beirut.
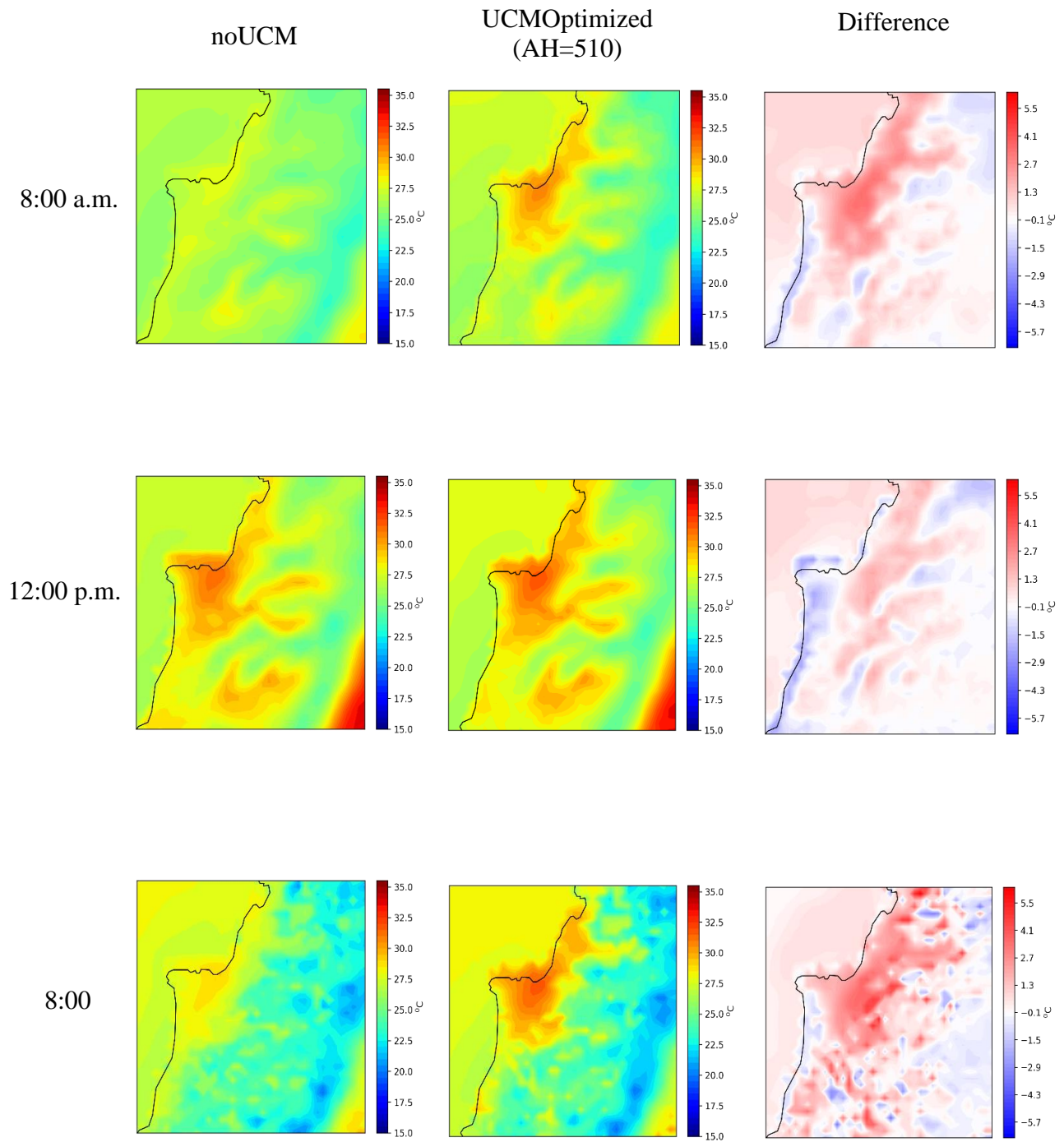
Figure 8: Heat maps showing the temperature distribution over domain (D3) for noUCM and UCMOptimized simulations as well as the difference between the two simulations at 8:00 a.m., 12:00 p.m., and 8:00 p.m. during July 2017
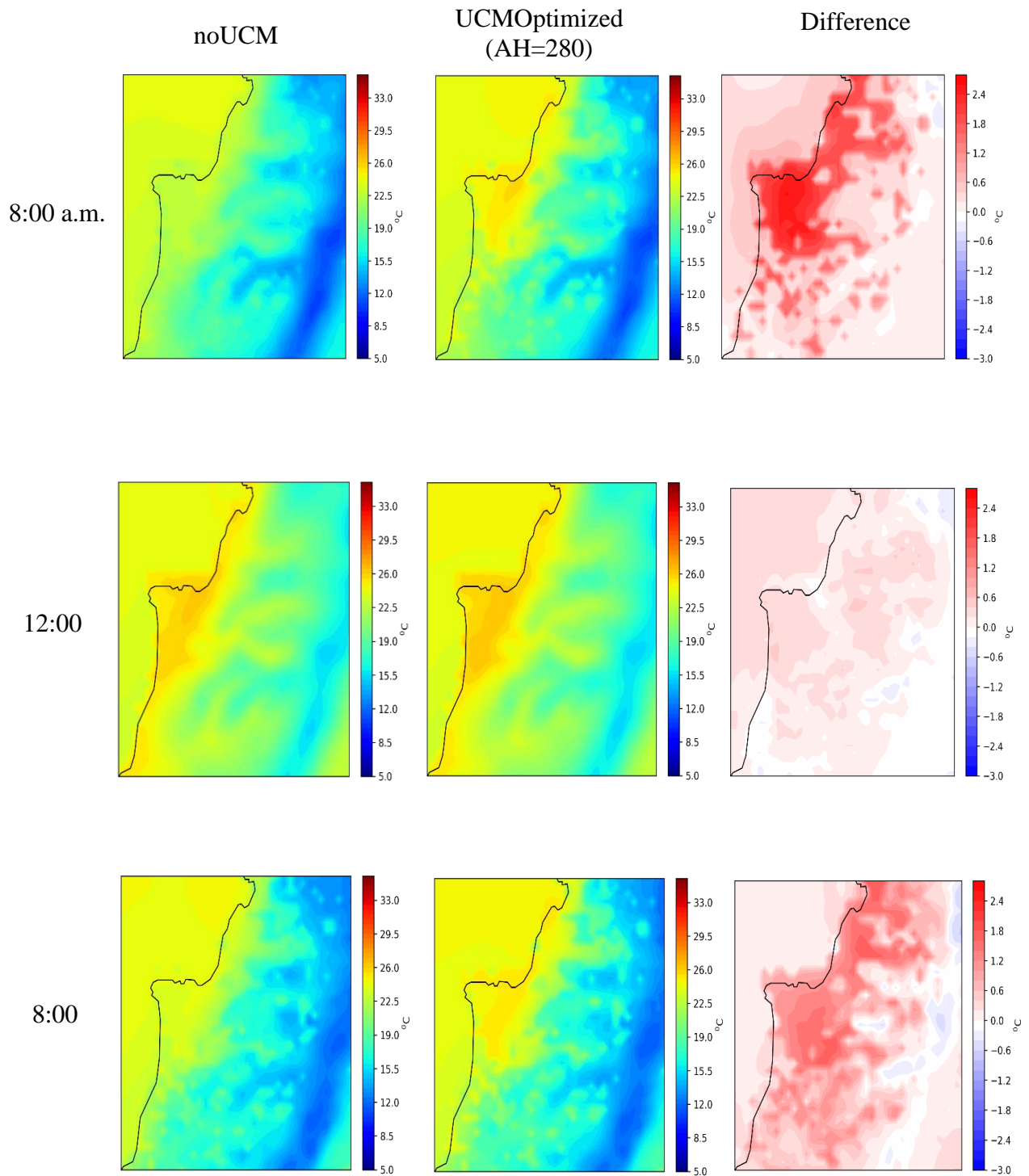
Figure 9: Heat maps showing the temperature distribution over domain (D3) for noUCM and UCMOptimized simulations as well as the difference between the two simulations at 8:00 a.m., 12:00 p.m., and 8:00 p.m. during October 2017
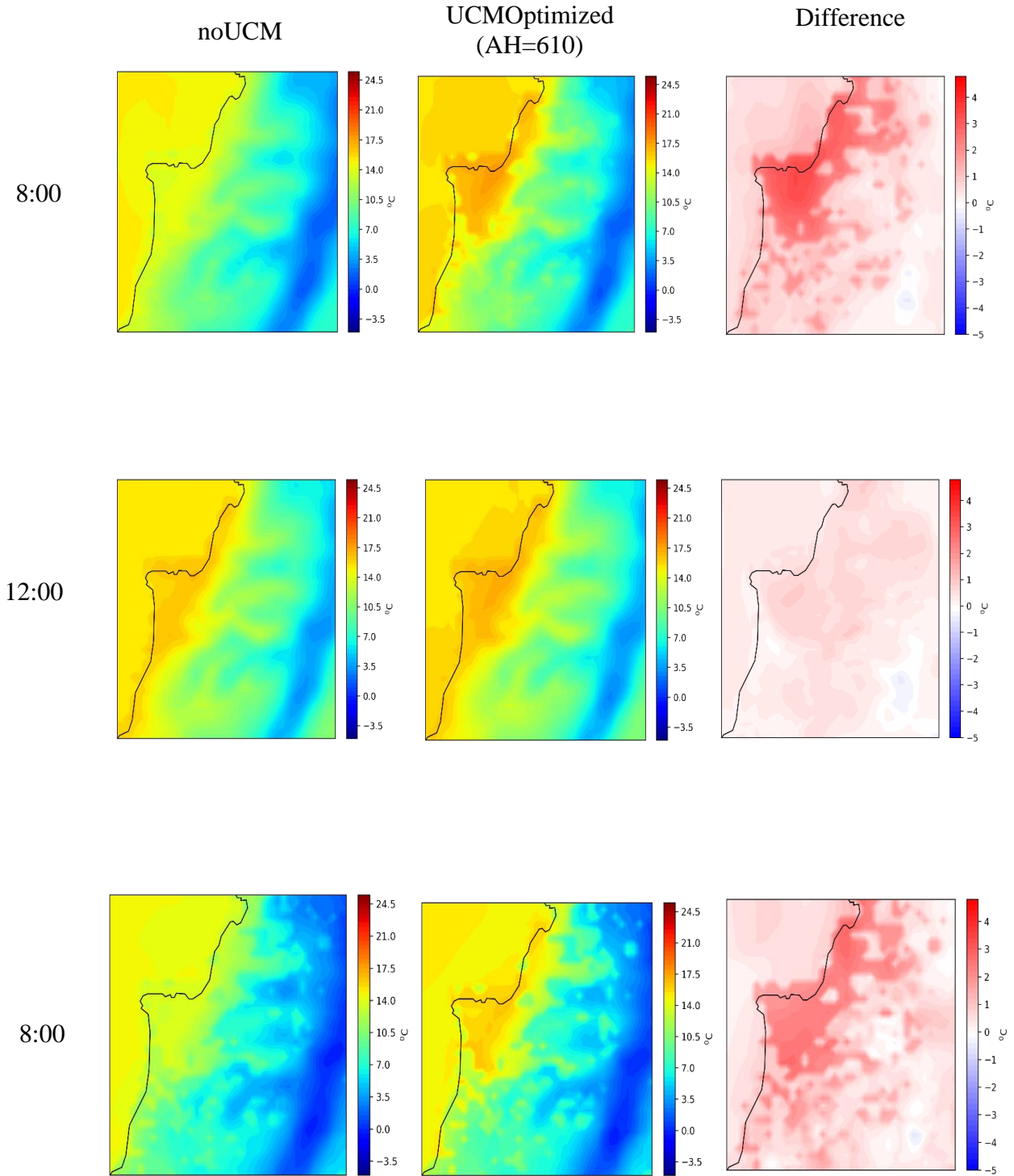
Figure 10: Heat maps showing the temperature distribution over domain (D3) for noUCM and UCMOptimized simulations as well as the difference between the two simulations at 8:00 a.m., 12:00 p.m., and 8:00 p.m. during January 2017
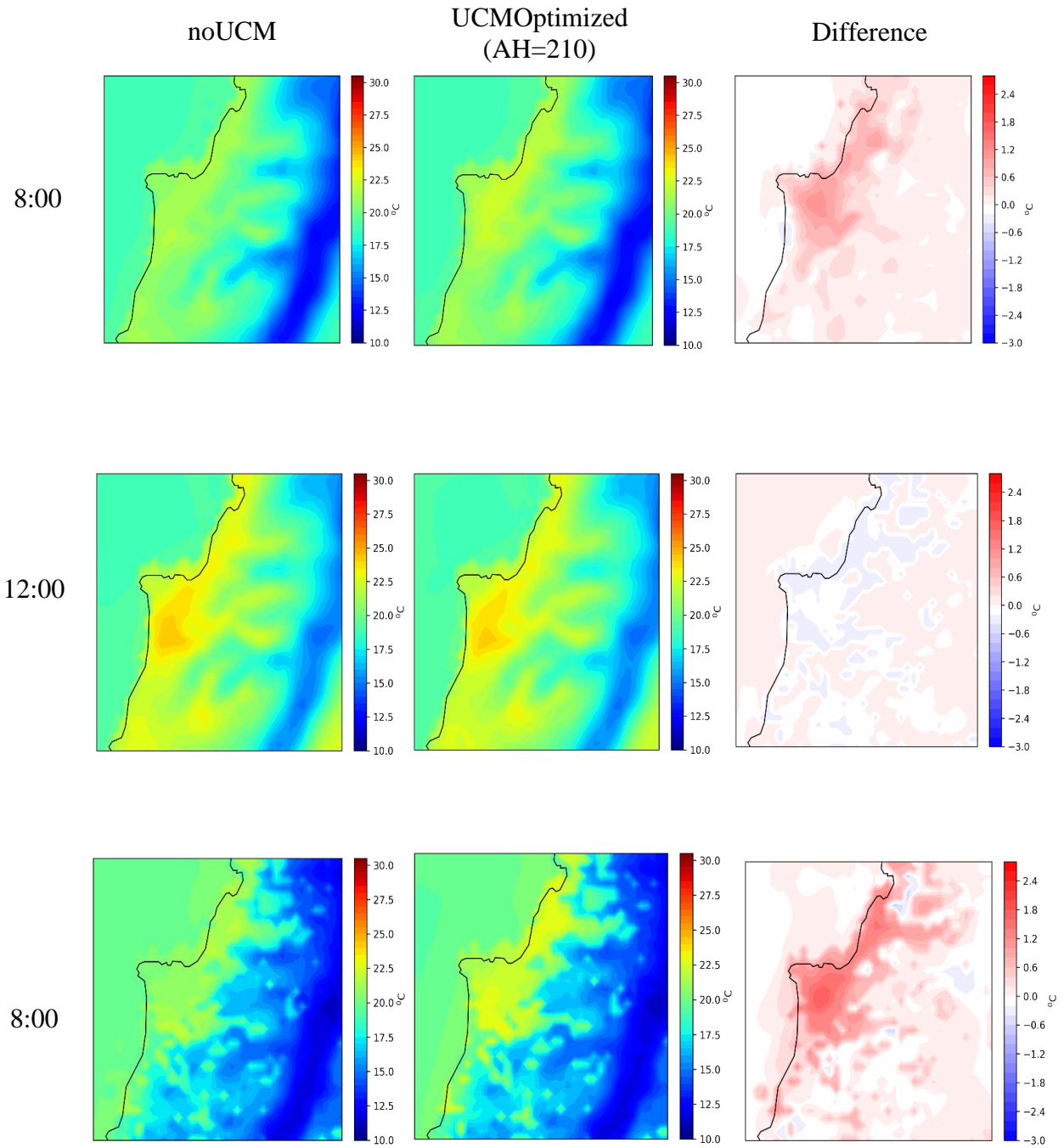
Figure 11: Heat maps showing the temperature distribution over domain (D3) for noUCM and UCMOptimized simulations as well as the difference between the two simulations at 8:00 a.m., 12:00 p.m., and 8:00 p.m. during April 2017

1. Predictive UCM

        To ensure that the optimized parameters are representative of Beirut not only during the year in which those parameters were tuned, the same parameters were used to predict the temperature during the same months but in the year 2018. Unlike the year 2017, the period chosen during 2018 was from the 2nd till the 8th (inclusive) of each month. Average simulated temperatures at Stn1 and Stn2 were compared with average observed temperatures at the same stations and plotted in Figure 12 (a – d). As can be seen, it is clear that UCMOptimized was capable of producing a temperature profile with a trend that is generally similar to the one that resulted from observations.

        A closer look at Figure 12 (a) clearly shows how the average predicted temperature profile followed the observed one during July 2018 where troughs and crests of both profiles were almost aligned at the same vertical cross – section. Statistical analysis showed that UCMOptimized resulted in an average error of -1.73 ^{0}C, RMSE of 2.05 ^{0}C, a NRMSE of 0.08, and a correlation coefficient of 0.64 which was the highest among all other simulations during the other months. During the first 3 days of October, the difference between simulated (UCMOptimized) and observed temperatures was about 1.6 ^{0}C while this difference reduced significanty during the remaining 4 days of the study period reaching an average of 0.3 ^{0}C. Moreover, statistical parameters for this month (Table 19) showed that values as low as -0.51 ^{0}C, 1.51 ^{0}C, and 0.06 were obtained for the MB, RMSE, and NRMSE respectively which are comparable to those obtained in 2017. Regarding January, although the resemblance of the simulated temperature profile to the observed one is not as strong as that obtained for the other months, which again, is explained by the fact that wind speed was included in the tuning process and January is characterized by high wind speeds with relatively high NRMSE, the

mean bias, RMSE, and NRMSE were comparable to those obtained in January 2017 especially the NRMSE where a difference of 0.03 was observed between the two years. As for the month of April, it is clearly shown how closely the simulated temperature profile followed the observed one except during the last simulation day where UCMOptimized underestimated the temperature. On average, statistical analysis yielded a mean bias of - 0.81 ^{0}C, RMSE of 2.27 ^{0}C, and a NRMSE of 0.11 which is very close to that obtained in April 2017 where a difference of 0.02 was observed.

Overall, UCM simulations that included optimized parameters performed better than those that included UCM with default parameters and those that did not include UCM at all. This is evident in Table 19 which shows that in terms of average error and with the exeption of January, UCMOptimized resulted in the least mean bias (in absolute value) with values of - 1.73 ^{0}C, - 0.51 ^{0}C, and - 0.81 ^{0}C during July, October, and April respectively. Moreover, the RMSE of UCMOptimized was the lowest compared to other UCM permutations during all months attaining values of 2.05 ^{0}C, 1.51 ^{0}C, 2.42 ^{0}C, and 2.27 ^{0}C during the months of July, October, January, and April respectively. Additionally, the NRMSE corresponding to UCMOptimized was the minimum compared to all other simulations during all months with the lowest value of 0.06 observed in October. Furthermore, a comparison between noUCM, UCMdefault, and UCMOptimized reveals that the latter produced improved temperature forecasts (i.e. less average error) by an average of 1.37 ^{0}C during July, 0.82 ^{0}C during October, and 0.93 ^{0}C during April when compared with noUCM and UCMdefault.

Average Simulated Temperature Versus Observed Temperature at All Stations During July 2018
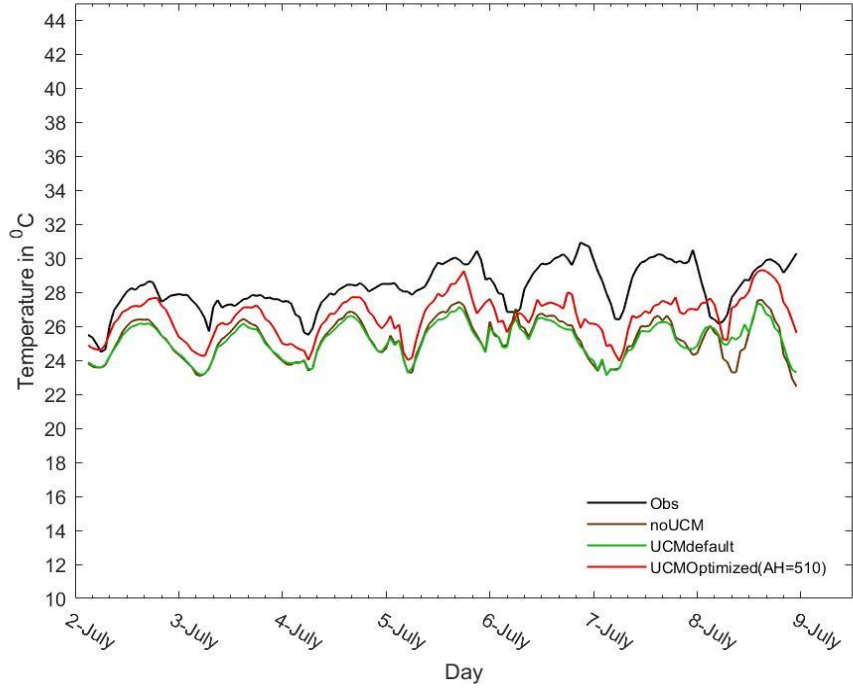
(a)

Average Simulated Temperature Versus Observed Temperature at All Stations During October 2018
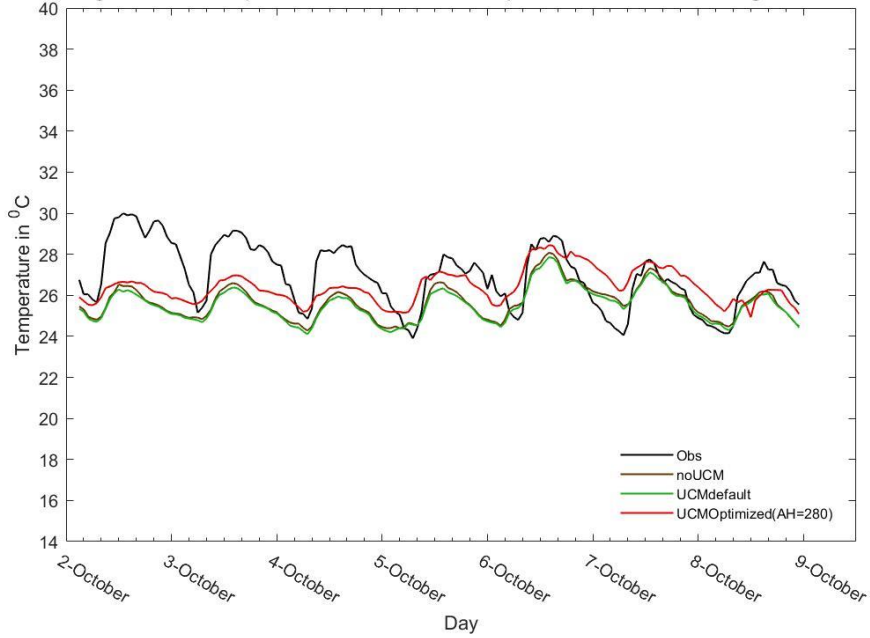
(b)

Average Simulated Temperature Versus Observed Temperature at All Stations During January 2018
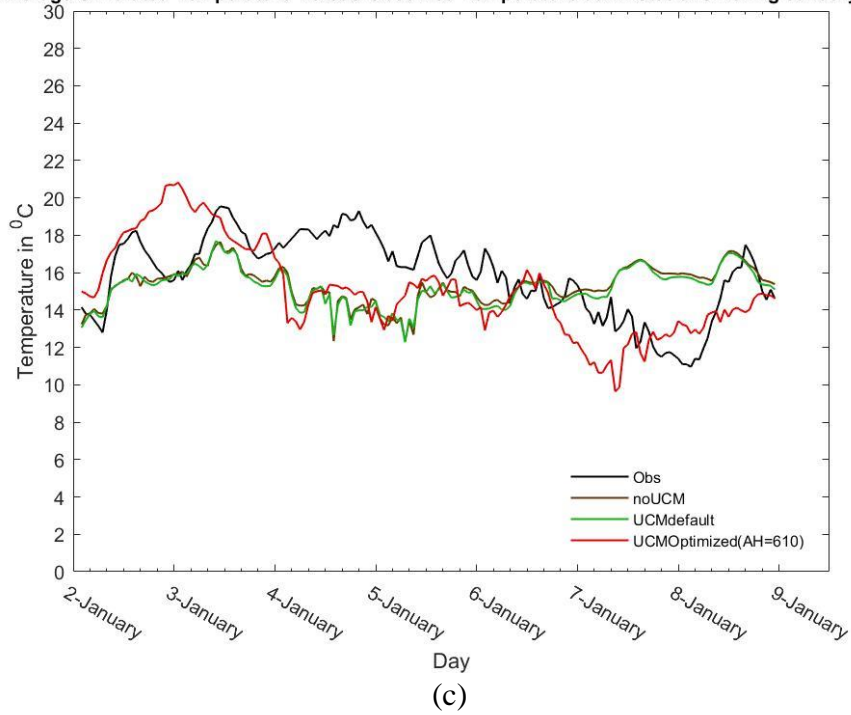
(c)

Average Simulated Temperature Versus Observed Temperature at All Stations During April 2018

(d)
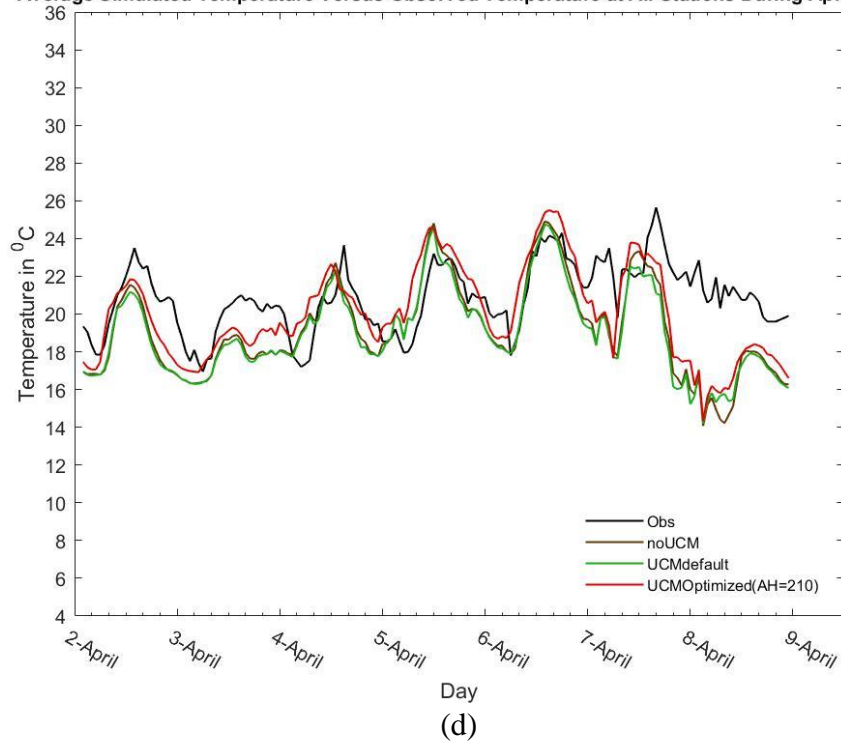
Figure 12: Comparison between average observed temperature and average predicted temperature with different permutations of UCM during (a) July (b) October (c) January and (d) April in the year 2018

58

Table 19: Statistical parameters for the average temperatures during July, October, January and April in the year 2018

		Average	Mean Bias	RMSE	NRMSE	CC
July	Obs	28.31				
	noUCM	25.24	-3.07	3.34	0.13	0.47
	UCMdefault	25.19	-3.12	3.36	0.13	0.47
	UCMOptimized(AH=510)	26.58	-1.73	2.05	0.08	0.64
October	Obs	26.93				
	noUCM	25.66	-1.27	1.80	0.07	0.56
	UCMdefault	25.54	-1.39	1.88	0.07	0.57
	UCMOptimized(AH=280)	26.42	-0.51	1.51	0.06	0.40
January	Obs	15.87				
	noUCM	15.33	-0.54	2.52	0.165	-0.10
	UCMdefault	15.20	-0.67	2.52	0.17	-0.06
	UCMOptimized(AH=610)	15.08	-0.79	2.42	0.161	0.51
April	Obs	20.83				
	noUCM	19.17	-1.66	2.66	0.14	0.56
	UCMdefault	19.01	-1.82	2.70	0.14	0.55
	UCMOptimized(AH=210)	20.02	-0.81	2.27	0.11	0.54

2. Further Check

Despite the fact that UCM optimum parameters were obtained by comparing simulated and observed variables, a further check – when possible – was performed to make sure that these parameters do make sense.

Regarding the roof albedo whose optimum value for Beirut was found to be equal to 0.03, a comparison with a map of roof albedos in Los Angeles created by the Berkely Lab Heat Island Group [32] showed very close values to those obtained as can be seen in Figure 13 below.
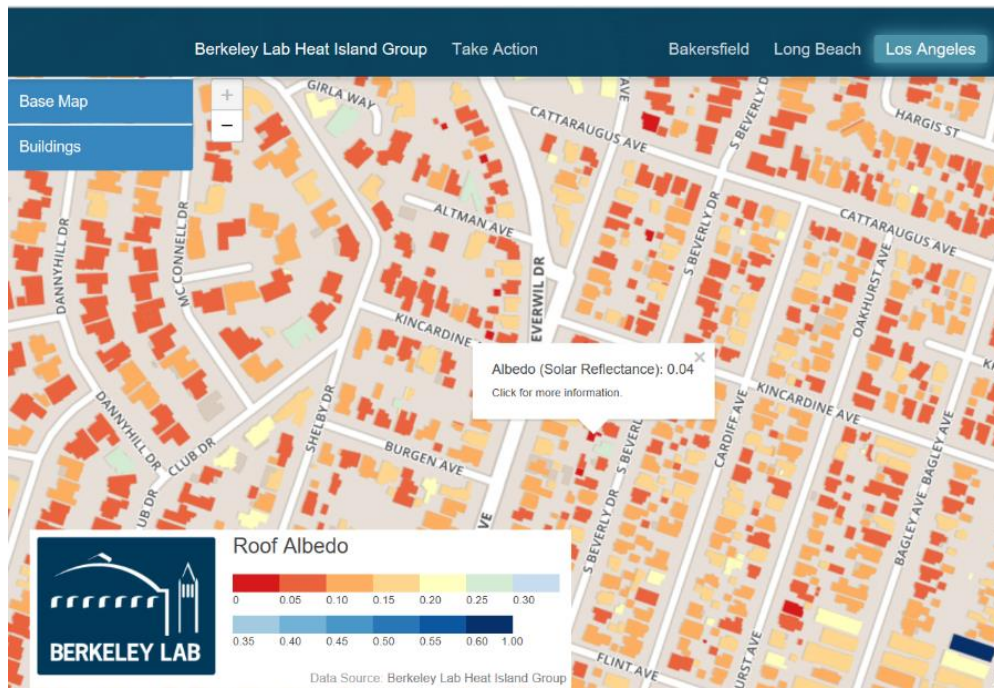
Figure 13: Map of roof albedos in Los Angeles (from [32])

As for the anthropogenic heat which was shown to be the most important parameter, fuel consumption in Lebanon during the year 2016 was used to get a rough estimate of the equivalent anthropogenic heat generated when this amount of fuel is burnt.

Table 20: Fuel imported by Lebanon in 2016. Units: Metric Ton

	Quantity (MT)	**% from total**
Gasoil	1,868,993	24%
Gasoline	2,081,812	27%
Diesel	1,615,898	21%
Fuel Oil	1,688,444	22%
LPG	238,730	3%
Kerozene	218,074	3%
Bitumen	91,841	1%
Total	7,803,792	100%

Table 20 shows Lebanese fuel imports in the year 2016 which was obtained through private communication with the Ministry of Environment. To calculate the heat generated by burning these amounts of fuel, the calorific value (CV) of all these fuel derivatives, except Bitumen, were obtained from a report published by the same ministry [33]. Having obtained the CV for each fuel type, it was then multiplied by the corresponding mass of the fuel to get the heat generated by burning the given amount of this fuel type as can be seen in Table 21. To get the value of the total AH which is represented in W/m^2, the resulting total energy of 333177.2 TJ/year was converted to J/s (W) assuming that heat is released for 12 hours per day. This calculated value (Q_L), however, represents AH released in the whole country. Hence, to get the fraction of this heat that is generated in Beirut only, the average annual consumption per capita in Lebanon [34] (Table 22) was used assuming that the numbers obtained reflect to some extent relative fuel consumption in each governorate. Consequently, to estimate the amount of AH generated in Beirut only (Q_B), the weighted – average of Q_L was calculated using the ratio for Beirut as a weight.

Table 21: Calculating a rough estimate of AH generated in Beirut

	CV (TJ/kton)	CV(TJ/ton)	E(TJ) = mass*CV
	43.33	0.04333	80983.46669
	44.8	0.0448	93265.1776
	43.33	0.04333	70016.86034
	40.19	0.04019	67858.56436
	47.31	0.04731	11294.3163
	44.75	0.04475	9758.8115
Total (TJ/year)			333177.20
Q_L(W)			21129959207.89
Q_B(W)			3423857347.83
Q(W/m²)			190.21

Table 22: Average annual consumption per capita (in 1000 LBP) in 2004 - 2005 (from [34])

Average Annual Consumption Per Capita (in 1000 LBP)		Population	Total Annual Consumption	Ratio[3]
Beirut	6514	390,503	2543736542	1.00
Mount Lebanon	4512	1,501,570	6775083840	2.66
Nabatieh	3924	768,709	3016414116	1.19
Bekaa	3385	471,209	1595042465	0.63
South	3007	401,197	1206399379	0.47
North	2532	221,846	561714072	0.22

Finally, Q_B was divided by the area of Beirut to get the amount of heat generated in Beirut per meter square (Q) which is representative of the average AH generated in the city. As can be seen, the estimated value of AH (190.21 W/m^2) is very close to the average value obtained by the tuning process (402.5 W/m^2). Despite this, the difference could be explained by the fact that the numbers used in the calculations represent only imported amounts of fuel that are recorded. If numbers corresponding to fuel reserves and fuel that is imported through the black market were available, the calculated value would undoubtedly be higher and consequently, a closer match would be expected.

---

[3] The ratio is the value corresponding to any governorate divided by that of Beirut.

B. Downscaling Results
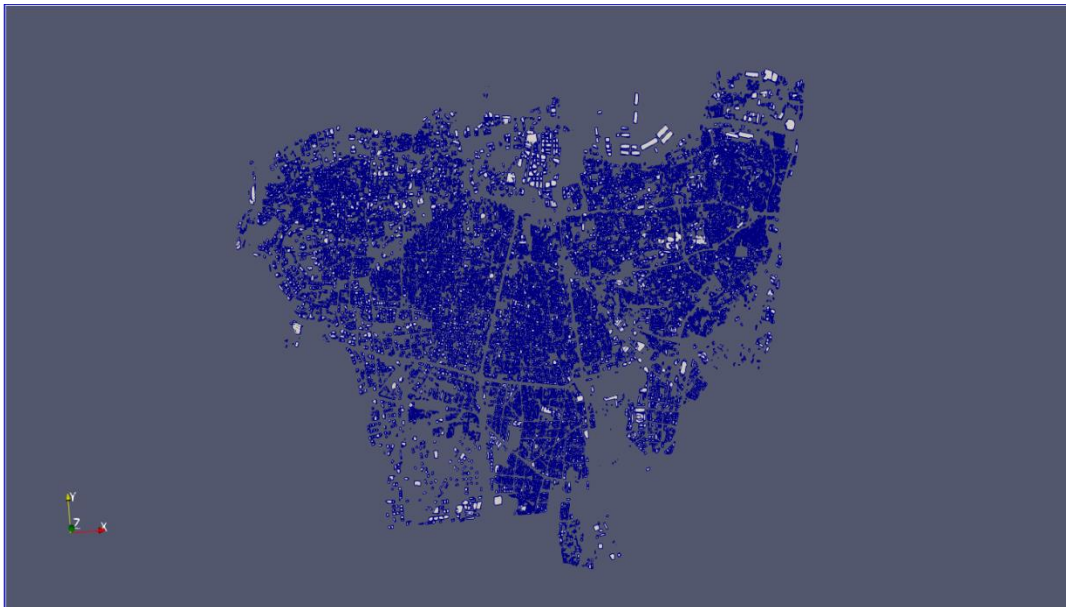
(a)
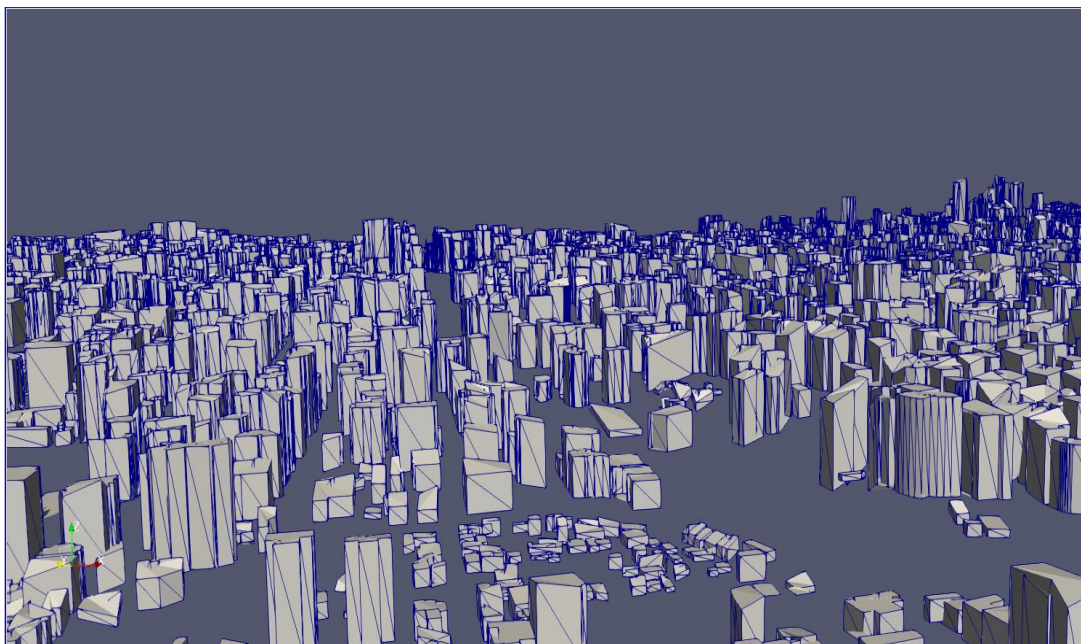
(b)

Figure 14: (a) Top view of digitized buildings in Beirut and (b) 3D view of the same buildings
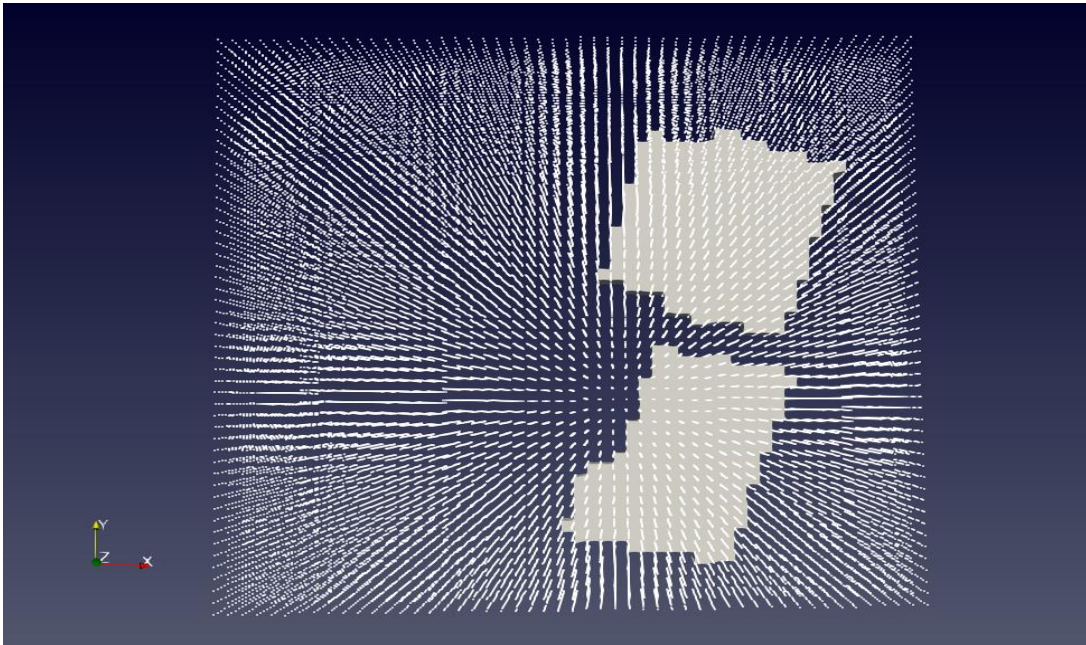
(a)
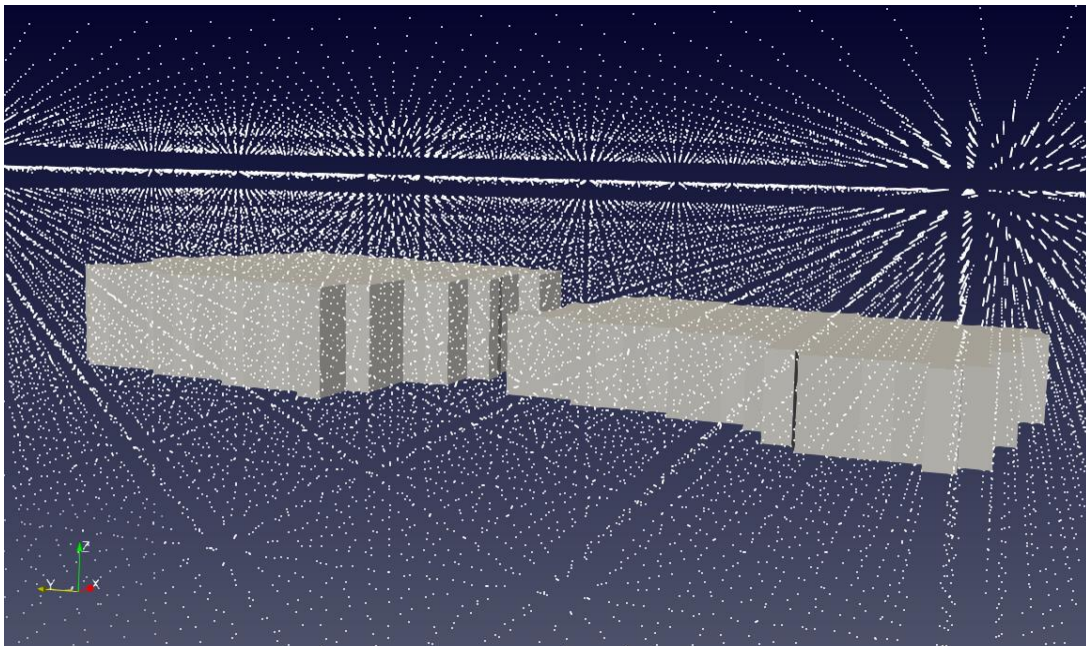
(b)

Figure 15: (a) Top view of the computational grid and the projected buildings and (b) 3D view of the grid and the projected buildings

64

As mentioned in the research statement, the work on downscaling is an initial effort which requires a lot more work; however, the work done so far will be presented. Figure 14 (a) and (b) shows the digitized buildings of Beirut from two different perspectives. Similarly, Figure 15 (a) and (b) show the computational grid on which calculations were performed. It also shows the two buildings that were projected onto the grid. It is noteworthy that the projection procedure caused the two buildings to be attached to each other, but they were separated apart so that the velocity field between them can be visualized.

As mentioned in the previous chapter, tuning of the parameters was performed so that a minimum total residual divergence was obtained. To get the optimum ratio, simulations at three different times during July 21st were performed where at each time, different ratios were considered. Figure 16, which shows the variation of the total residual divergence as a function of the alpha ratio squared, reveals that a maximum reduction in the divergence was achieved for alpha ratio of 1 at all 3 times indicating identical values of α_1 and α_3.

(a)
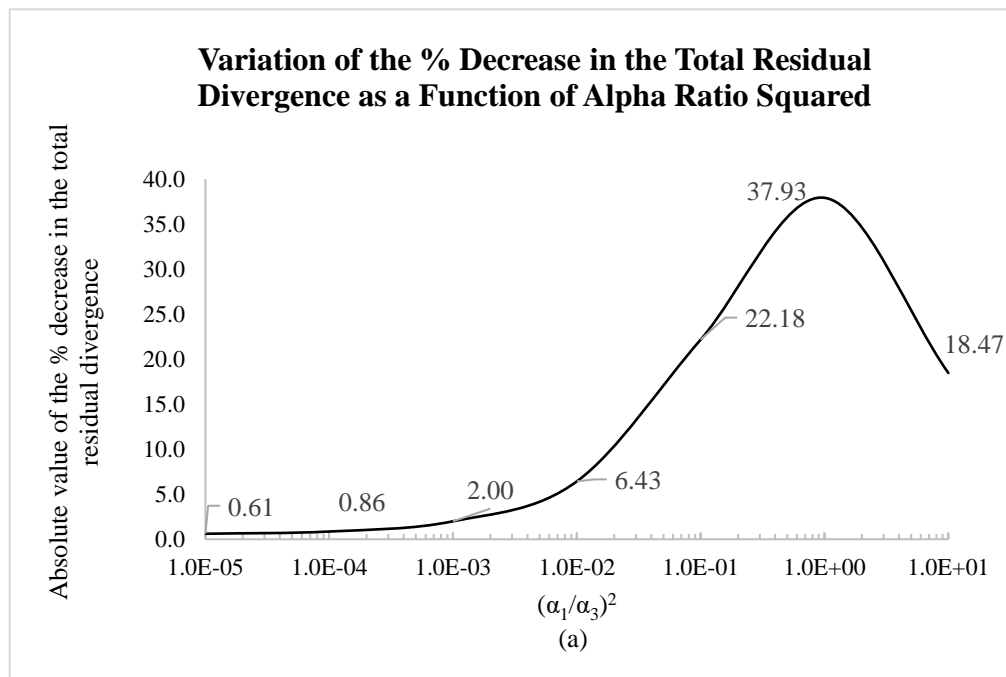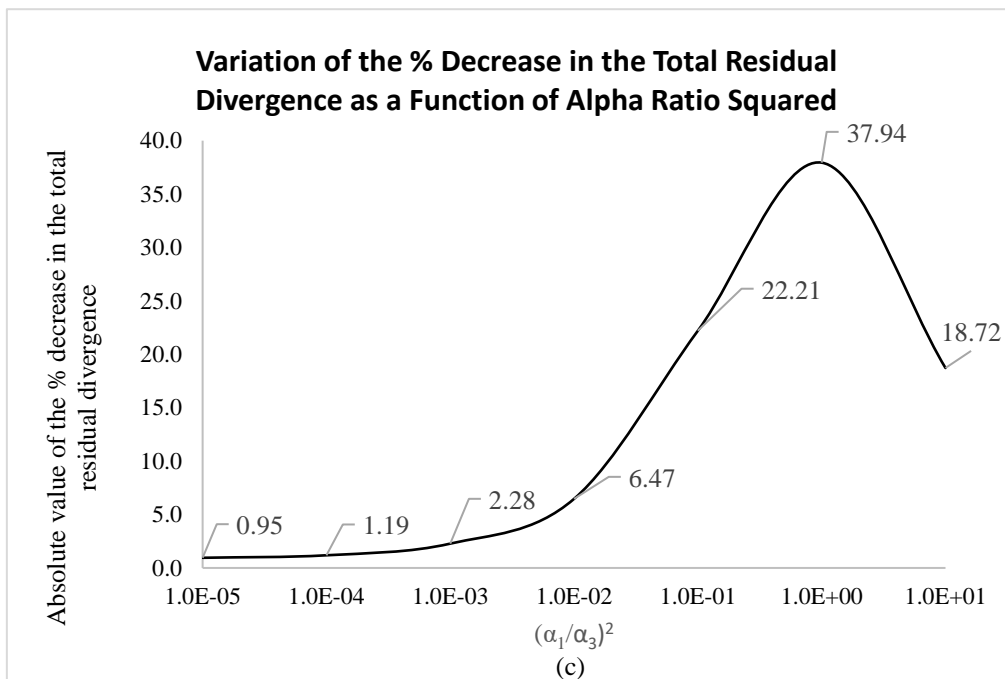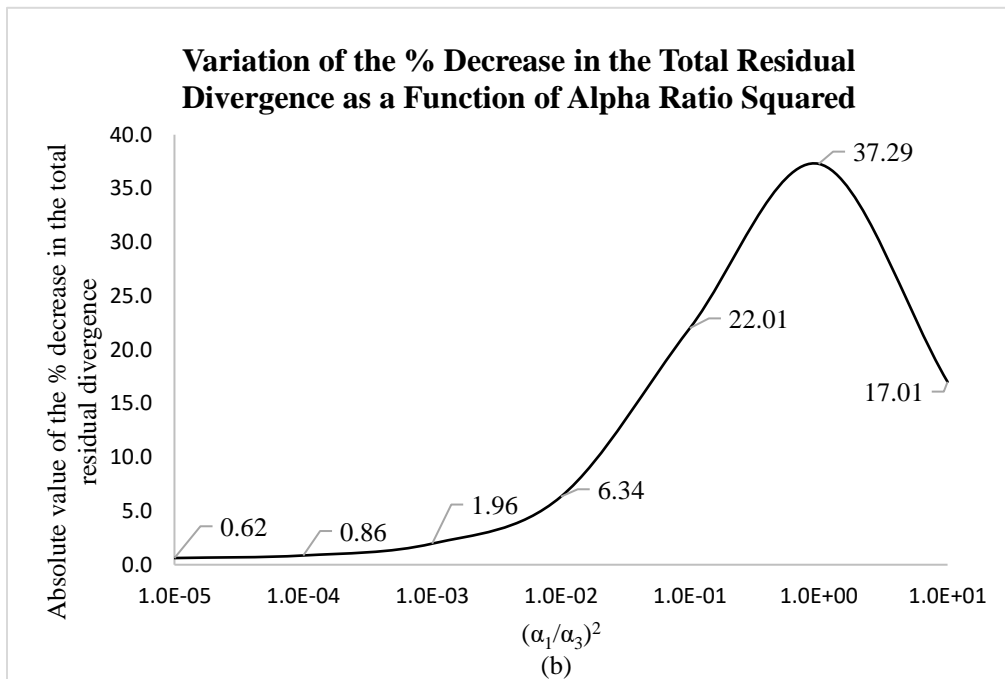
Figure 16: Variation of the percentage decrease (in absolute value) in the total residual divergence as a function of $(\alpha_1/\alpha_3)^2$ at (a) 8:00 a.m. (b) 12:00 p.m. and (c) 8:00 p.m. in July 21, 2017
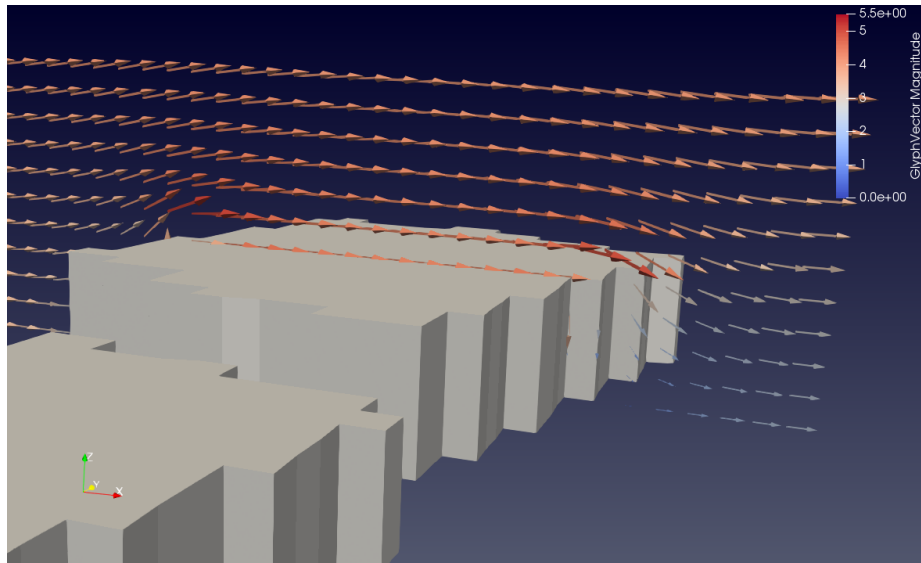
The following figures show the calculated adjusted velocity field, with $\left(\dfrac{\alpha_1}{\alpha_3}\right)^2 = 1$

at different cross – sections of the computational domain in July 21st, 2017 at 12:00 p.m.
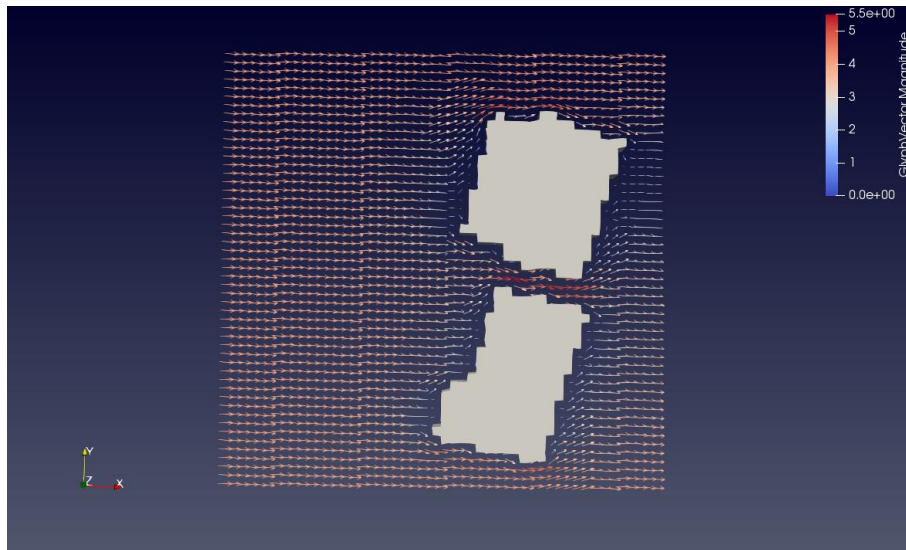
(a)
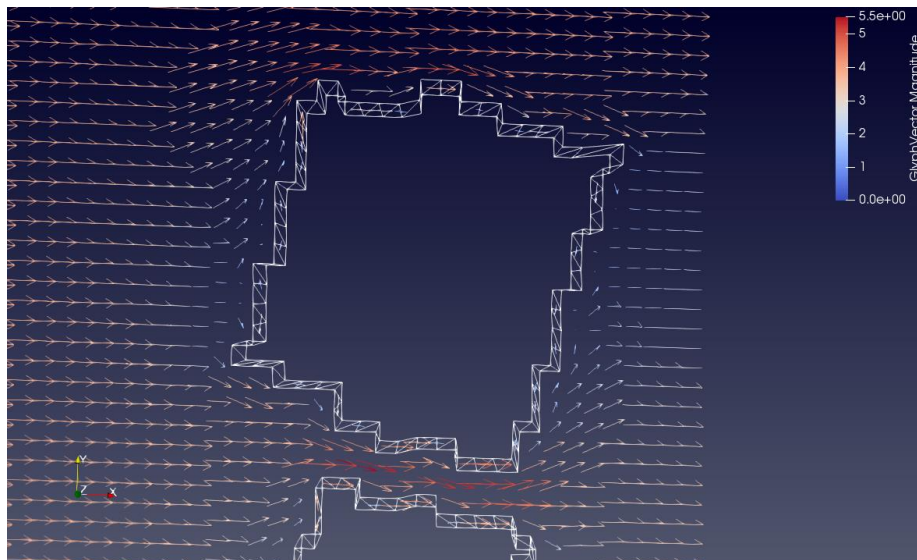
(b)

(c)

Figure 17: The adjusted flow field at (a) & (b) a horizontal slice and (c) a vertical slice
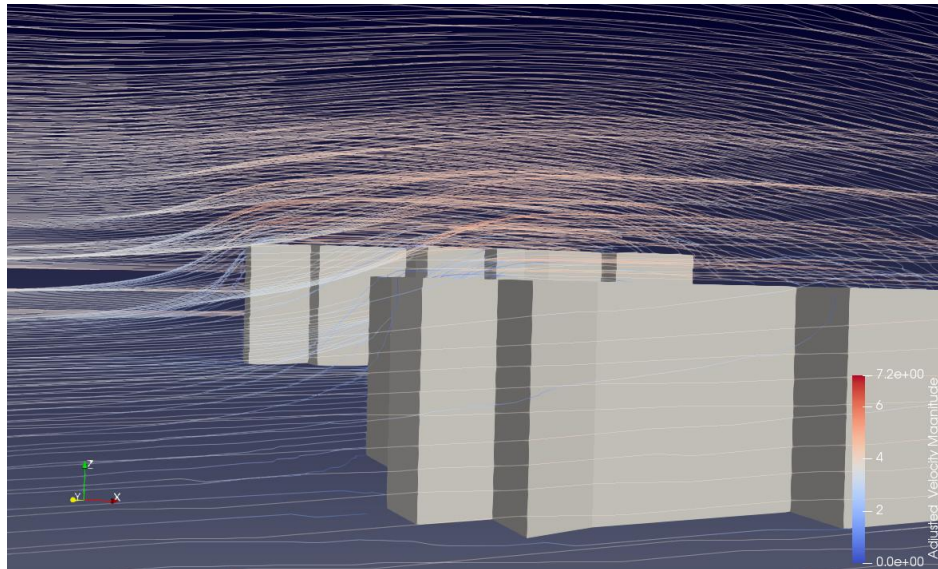
Figure 18: Streamlines over the projected buildings

CHAPTER IV

CONCLUSION AND FUTURE WORK

This work represents the first effort in Lebanon in which a weather forecasting model was coupled with an urban canopy model and urban parameters were tuned to reflect actual weather conditions, represented by temperature, in Beirut city. Furthermore, an initial effort of downscaling the velocity field from WRF's scale (1 km) to the pedestrian scale (1 m) while satisfying mass conservation was presented.

As a future work, WRF-UCM could be extended further by:

1. performing a sensitivity study on different urban parameters such as the roof and wall, albedo, AH, and urban fraction to study the relative effect of higher/lower values on the formation of the urban heat island in Beirut

2. performing pollution dispersion simulations by coupling chemistry with WRF-UCM using the tuned parameters

In terms of downscaling, more work can be done in the future such as:

1. studying the sensitivity of the solution to different grid dimensions and to check whether a grid – independent solution can be obtained or not

2. obtaining a solution using other atmospheric stability conditions because in this work, the exponent of the power law was based on neutral atmospheric conditions

3. Using another method, such as finite differencing, and comparing its results with those obtained using the finite element method

4. considering a larger domain with more buildings and studying its relative effect on the alpha ratio

REFERENCES

[1] Beirut [Online]. Available:
     http://academic.eb.com.ezproxy.aub.edu.lb/levels/collegiate/article/Beirut/109399

[2] UN-Habitat. (2014, 2017). *Lebanon – Urban Issues*. Available:
     https://unhabitat.org/lebanon/lebanon-urban-issues/

[3] M. A. Helou, "Impact of distributed urban generators on household exposure to
     carcinogenic airborne particles during rolling blackout episodes," Masters,
     Mechanical Engineering, American University of Beirut, AETJ ET:5674:c.1
     2012.

[4] W. C. Skamarock *et al.*, "A description of the Advanced Research WRF Version 3,"
     2008.

[5] J. K. S. Ching, "A perspective on urban canopy layer modeling for weather, climate and
     air quality applications," *Urban Climate,* vol. 3, no. Supplement C, pp. 13-39,
     2013/05/01/ 2013.

[6] M. Tewari, F. Chen, and H. Kusaka, *Implementation and Evaluation of a Single –Layer
     Urban Canopy Model in WRF/Noah*. 2006.

[7] NCAR. *THE WEATHER RESEARCH & FORECASTING MODEL*. Available:
     https://www.mmm.ucar.edu/weather-research-and-forecasting-model

[8] Y. Liu, F. Chen, T. Warner, and J. Basara, "Verification of a Mesoscale Data-
     Assimilation and Forecasting System for the Oklahoma City Area during the Joint
     Urban 2003 Field Project," *Journal of Applied Meteorology and Climatology,* vol.
     45, no. 7, pp. 912-929, 2006.

[9] H. Kusaka, H. Kondo, Y. Kikegawa, and F. Kimura, "A Simple Single-Layer Urban
     Canopy Model For Atmospheric Models: Comparison With Multi-Layer And Slab
     Models," *Boundary-Layer Meteorology,* journal article vol. 101, no. 3, pp. 329-358,
     December 01 2001.

[10] H. Kusaka and F. Kimura, "Thermal Effects of Urban Canyon Structure on the Nocturnal Heat Island: Numerical Experiment Using a Mesoscale Model Coupled with an Urban Canopy Model," *Journal of Applied Meteorology,* vol. 43, no. 12, pp. 1899-1910, 2004/12/01 2004.

[11] A. Sharma, H. J. S. Fernando, A. F. Hamlet, J. J. Hellmann, M. Barlage, and F. Chen, "Urban meteorological modeling using WRF: a sensitivity study," *International Journal of Climatology,* vol. 37, no. 4, pp. 1885-1900, 2017/03/01 2016.

[12] A. Martilli, A. Clappier, and M. W. Rotach, "An Urban Surface Exchange Parameterisation for Mesoscale Models," *Boundary-Layer Meteorology,* journal article vol. 104, no. 2, pp. 261-304, August 01 2002.

[13] F. Chen *et al.*, "The integrated WRF/urban modelling system: development, evaluation, and applications to urban environmental problems," *International Journal of Climatology,* vol. 31, no. 2, pp. 273-288, 2011.

[14] C. F. Ratto, R. Festa, C. Romeo, O. A. Frumento, and M. Galluzzi, "Mass-consistent models for wind fields over complex terrain: The state of the art," *Environmental Software,* vol. 9, no. 4, pp. 247-268, 1994/01/01/ 1994.

[15] R. A. Pielke, *Mesoscale Meteorological Modeling* (International Geophysics Series). San Diego: Academic Press, 2002.

[16] C. A. Sherman, "A Mass-Consistent Model for Wind Fields over Complex Terrain," *Journal of Applied Meteorology,* vol. 17, no. 3, pp. 312-319, 1978/03/01 1978.

[17] T. Kitada, A. Kaki, H. Ueda, and L. K. Peters, "Estimation of vertical air motion from limited horizontal wind data—a numerical experiment," *Atmospheric Environment (1967),* vol. 17, no. 11, pp. 2181-2192, 1983/01/01/ 1983.

[18] G. R. Carmichael and L. K. Peters, "The Transport, Chemical Transformation, and Removal of SO2 and Sulfate in the Eastern United States," in *Studies in Environmental Science*, vol. 8, M. M. Benarie, Ed.: Elsevier, 1980, pp. 31-36.

[19] S. D. Reynolds, P. M. Roth, and J. H. Seinfeld, "Mathematical modeling of photochemical air pollution—I: Formulation of the model," *Atmospheric Environment (1967),* vol. 7, no. 11, pp. 1033-1061, 1973/11/01/ 1973.

[20] L. K. Peters and A. A. Jouvanis, "Numerical simulation of the transport and chemistry of CH4 and co in the troposphere," *Atmospheric Environment (1967),* vol. 13, no. 10, pp. 1443-1462, 1979/01/01/ 1979.

[21] Y. Sasaki, "An objective analysis based on the variational method," *Journal of the Meteorological Society of Japan. Ser. II,* vol. 36, no. 3, pp. 77-88, 1958.

[22] Y. Sasaki, *Some basic formalisms in numerical variational analysis*. Citeseer, 1970.

[23] M. H. Dickerson, "MASCON—A mass consistent atmospheric flux model for regions with complex terrain," *Journal of Applied Meteorology,* vol. 17, no. 3, pp. 241-253, 1978.

[24] R. Mathur and L. K. Peters, "Adjustment of wind fields for application in air pollution modeling," *Atmospheric Environment. Part A. General Topics,* vol. 24, no. 5, pp. 1095-1106, 1990.

[25] J. M. Forthofer, B. W. Butler, and N. S. Wagenbrenner, "A comparison of three approaches for simulating fine-scale surface winds in support of wildland fire management. Part I. Model formulation and comparison against measurements," *International Journal of Wildland Fire,* vol. 23, no. 7, pp. 969-981, 2014.

[26] "NCEP GFS 0.25 Degree Global Forecast Grids Historical Archive," ed. Boulder, CO: Research Data Archive at the National Center for Atmospheric Research, Computational and Information Systems Laboratory, 2015.

[27] M. Tewari, F. Chen, H. Kusaka, and S. Miao, "Coupled WRF/Unified Noah/urban-canopy modeling system," *Ncar WRF Documentation, NCAR, Boulder,* vol. 122, 2007.

[28] A. Waked *et al.*, "Modeling air pollution in Lebanon: evaluation at a suburban site in Beirut during summer," *Atmospheric Chemistry and Physics,* vol. 13, no. 12, pp. 5873-5886, 2013.

[29] Available: www.wunderground.com

[30] D. L. Logan, *A first course in the finite element method*. 2017.

[31] Order of Engineers and Architects of Beirut and LIBNOR, "THERMAL STANDARD FOR BUILDINGS IN LEBANON," 2010.

[32] Berkeley Lab Heat Island Group. Available: https://albedomap.lbl.gov/

[33] Ministry of Environment, "NATIONAL GREENHOUSE GAS INVENTORY REPORT AND MITIGATION ANALYSIS FOR THE ENERGY SECTOR IN LEBANON," 2015.

[34] United Nations Development Programme (UNDP), "Poverty, Growth & Inequality in Lebanon," 2007.